Elsevier Editorial System(tm) for Cell
Manuscript Draft

Manuscript Number: CELL-D-11-00919R1

Title: Gene expression is a circular process

Article Type: Research Article

Keywords: 5' to 3' mRNA decay; transcription; regulation of gene expression; XRN1

Corresponding Author: Professor Mordechai Choder, Ph.D.

Corresponding Author's Institution:

First Author: Gal Haimovich

Order of Authors: Gal Haimovich; Sebastien Z Causse; Daniel Medina; Gonzalo Millán-Zambrano; Oren Barkai; José E Pérez-Ortín; Sebastián Chávez; Xavier Darzacq; Mordechai Choder

Abstract: Maintaining the proper level of mRNAs is a key aspect in the regulation of gene expression. The balance between mRNA synthesis and decay determines these levels. Using a whole-genome analysis, we demonstrate that most yeast mRNAs are degraded by the 5' to 3' pathway (the "decaysome"), as proposed previously. Unexpectedly, the level of these mRNAs is highly robust to perturbations in this major pathway, as defects in various decaysome components lead to down-regulation of transcription. Moreover, these components shuttle between the cytoplasm and the nucleus, in a manner dependent on proper mRNA degradation; in the nucleus, they associate with chromatin and directly stimulate transcription initiation and elongation. Hence, the major decaysome has a dual role in maintaining mRNA levels. Significantly, proper import of some decaysome components seems to play a key role in coupling the two functions. Gene expression process is therefore circular, whereby the hitherto first and last stages are interconnected.

Suggested Reviewers:

Opposed Reviewers:

*Cover Letter (required for ALL submissions)

March 5, 2012

Kara L Cerveny, Ph.D.
Scientific Editor, Cell
Cell Press
600 Technology Square
Cambridge, MA 02139

Dear Kara,

I would like to thank you and the three reviewers for considering our manuscript for publication in Cell.

We appreciate the reviewer's very constructive comments and suggestions. We have given serious consideration to all points brought up by yourself and the reviewers and have revised our manuscript accordingly.

During the revision period, an additional group, led by Prof. Chávez, who specialized in utilizing whole genome analyses for studying transcription elongation, joined the team. In the last several months, the team (which includes now 4 groups from across Europe) has made substantial progress. Using various multidisciplinary approaches, we have made progress in unraveling the mechanism underlying the decaysome's role in transcription. In particular we focused on two key issues. First, we demonstrate that the decaysome acts both in initiation and the last stages of elongation in a TFIIS-independent mechanism. Second, we show that the nuclear import of the decaysome, which occurs normally only if the mRNA is degraded from 5' to 3', is a key regulatory step linking mRNA degradation in the cytoplasm and transcription activation in the nucleus. In addition, we include a number of experiments, suggested by the reviewers, which improved the paper significantly. In response to some comments of the reviewers, we also clarified several points that were counter-intuitive and not easily explained.

Overall, we performed a number of additional experiments. The new data are presented in the following Figure panels: 1C; 4B-D; 5C; 6A-C; 7A-C, S1D-E; S5C-D & F and S6 and in Tables S1, S2, S4, S5 and S6.

Below, please find our point-by-point responses to the issues raised by the reviewers and a description of the changes that we made in the manuscript.

Overall, we believe that our manuscript has been significantly improved and strengthened. We hope that our revised manuscript satisfies the requests of the reviewers, and that you will find it suitable for publication in Cell.

Sincerely yours,

Mordechai Choder

*Abstract (required for ALL submissions)

ABSTRACT

Maintaining the proper level of mRNAs is a key aspect in the regulation of gene expression. The balance between mRNA synthesis and decay determines these levels. Using a whole-genome analysis, we demonstrate that most yeast mRNAs are degraded by the 5' to 3' pathway (the "decaysome"), as proposed previously. Unexpectedly, the level of these mRNAs is highly robust to perturbations in this major pathway, as defects in various decaysome components lead to down-regulation of transcription. Moreover, these components shuttle between the cytoplasm and the nucleus, in a manner dependent on proper mRNA degradation; in the nucleus, they associate with chromatin and directly stimulate transcription initiation and elongation. Hence, the major decaysome has a dual role in maintaining mRNA levels. Significantly, proper import of some decaysome components seems to play a key role in coupling the two functions. Gene expression process is therefore circular, whereby the hitherto first and last stages are interconnected.

RESPONSES TO REVIEWERS

Reviewer 1

We would like to thank Reviewer 1 for his/her thorough review and many constructive comments that helped us improve our manuscript. In response to his/her comments, we have performed the following experiments and clarifications in the text:

Major points:

1. In response to this comment, we determine mRNA half-lives (HL) on a whole genome scale. As shown in Fig 1C and Table S1 the levels of most mRNAs are lower in the Δ*xrn1* mutant, relative to WT. We found no correlation between changes in HL and changes in these levels. Thus the balance between mRNA synthesis and decay is maintained, no matter how strong the effect of deleting XRN1 on HL is. In fact, this balance is somewhat compromised in the absence of *XRN1* because most levels are lower in the mutant compared to WT.
   To address Reviewer 1's specific comment, I should indicate that even in those mRNAs whose decay rates change substantially, the mRNA level was maintained or decreased (see Fig 1C and Table S1).
2. In the first version of this paper, we had two replicas of GRO data, which limited our mode of normalization. In order to improve the normalization, we performed a third replicate of the experiment. This allowed us, then, to analyze the results using a "median absolute deviation" procedure (ArrayStat software), as we have done previously (Garcia-Martinez et al, 2004; 2011). Using this much better dataset, there was no need to normalize to rRNA. Instead, based on our long-term experience (op. cit.), we surmised that analyzing the 3 strains simultaneously (WT Δ*xrn1* and *xrn1*^{D208A}), using the same reagents and conditions, should produce only random noise that can be (mostly) corrected by the statistical analysis. Total Pol II TR in Δ*xrn1* and *xrn1*^{D208A} showed a clear decrease with regard to WT in every repeat (Figs. 1D & S1C). Using this approach, the decrease was in fact stronger than that shown in our previous version of the paper, in which we used rRNA normalization. To normalize the mRNA amounts (RA) data, we first evaluated the total mRNA/cell by using a capillary electrophoresis cartridge (Experion, BioRad) that can separate rRNA signals (5S, 18S, 25S and tRNA) from the rest. We assumed that the area covered in between 5S and 18S peaks is mainly mRNA (levels of non-coding RNAs are far below those of mRNAs, see for example Churchman and Weissman 2011). We found that this area is well measured (there was very low variability between technical replicates and low variability between samples from biological replicates). See Table S6. Therefore, we took that value as mRNA/total RNA. Then we multiplied it by the total RNA/total cell volume. In this way we obtained a specific "mRNA concentration" for each strain. Using this RA normalization method, we found that total mRNA/cell does not vary much between strains (Fig. 1C). This observation

reinforces the conclusion that, upon *xrn1* disruption, mRNA HL and TR change in a compensatory manner.

3. It was recently shown that *GAL10* mRNA half-life under galactose growth conditions is in the order of 20 min (Munchel et al., 2011), which is within the time-frame of our experiment. We agree that the mRNA stability can change temporarily during the shift from raffinose to galactose and it may be longer than 20 min. Nevertheless, our GRO (Fig. 1D) results demonstrate that the Δ*xrn1* cells are, indeed, defective in transcription. We emphasized this point in the section that discusses Fig. 2 (see pages 6 and 7, blue sentences). Moreover, defective transcriptional capacity of Δ*xrn1* cells can be deduced also from Pol-II ChIP (Fig. 6C), Ser2 phosphorylation (Fig. 6C) and FISH (Fig. 3 and S3).
4. Several experiments performed independently by the Choder and Chávez groups, consistently demonstrated that Xrn1 is associated also with intergenic regions, unlike Pol II. Specifically, ChIP Xrn1 signals of intergenic amplicons were at least 2-fold stronger that those of No-TAP. We do not understand why Xrn1, unlike Rpb3, gives reproducible ChIP signals in the intergenic regions. Maybe this reflects the possibility that Xrn1 remains bound to chromatin that has a history of transcription and that many intergenic regions have such a history due to transcription of non-coding RNA. Be it as it may, equally reproducible was the ≥2-fold increase of ORFs signals relative to the intergenic ones (amplicon 115 of PMA1 gave a signal that was 7.1±2.6 fold higher than the "no-tag" signal). Furthermore, in the revised manuscript, we show that the ChIP signal of Xrn1-TAP along the *GAL1* ORF is increased when the cells are stimulated by galactose (Fig 5C).

Minor point: We agree with Reviewer 1 that this figure is both interesting and confusing. Since this figure is a snapshot, we suspect that all cells in the population cannot sustain a normal mRNA level; it fluctuates up and down like the temperature controlled by a bad thermostat. I agree with the Reviewer that this issue deserves future in depth study and decided to remove it from this paper. Please see also item #3 in our response to Reviewer 3.

Reviewer 1 suggested to provide a clear take home message from each experiment. In the revised manuscript we tried our best to do it.

Reviewer 2

We would like to thank Reviewer 2 for viewing our finding as "potentially ground – breaking" and for his/her thorough review and many constructive comments that helped us improve our manuscript. In response to his/her comments, we have performed the following experiments and clarifications in the text:

Major points:

1) Reviewer 2 raised several issues and suggestions on how to consolidate the direct role of decay factors in transcription.
   a) Several experiments performed independently by the Choder and Chávez groups, consistently demonstrated that Xrn1p is associated also with intergenic regions, unlike Pol II. Specifically, Xrn1 ChIP signals of intergenic amplicons were at least 2-fold stronger that those of No-TAP. We do not understand why Xrn1, unlike Rpb3, gives reproducible ChIP signals in the intergenic regions. Maybe this reflects the possibility that Xrn1 remains bound to chromatin that has a history of transcription and that many intergenic regions have such a history due to transcription of non-coding RNA. Be it as it may, equally reproducible was the ≥2-fold increase of ORFs signals relative to the intergenic ones. Reviewer 2 recommended examining whether Xrn1p dependence on transcription is correlated with chromatin association. In the revised manuscript, we show that the ChIP signal of Xrn1-TAP along the *GAL1* ORF is increased when the cells are stimulated by galactose (Fig 5C). Moreover, as recommended by Reviewer 2, we compared Dcp2-TAP ChIP in WT with the signal obtained in an $xrn1^{D208A}$ background. Indeed, the ChIP signal in this mutant background is significantly lower than in WT cells (Fig S5D). Finally, in response to Reviewer 2's suggestion, we performed ChIP in the presence of RNase and we show that the ChIP signal is not decreased (Fig S5C). All these new data reinforce our view that some DFs are associated with chromatin in a functional manner.
   b) We embraced reviewer 2's idea of creating a second mutation in *XRN1* to challenge our hypothesis that the $xrn1^{D208A}$ mutant is trapped in the cytoplasm because it binds mRNA without degrading it. Recently, the structure of Xrn1 was published and several amino-acids were shown to be critical for binding the 5'-P end region of the decapped mRNA (e.g. Arg101 and His41). We therefore introduced a second mutation (R101G) into $Xrn1^{D208A}$ in order to abolish mRNA binding. Obviously and importantly, this mutation does not rescue mRNA decay. Strikingly, this mutation recovered Dcp2 import (Fig 4C) and improved the ability of the cells to transcribe GAL genes, (compare transcriptional performance of $xrn1^{D208A}$ cells with that of $xrn1^{D208A,R101G}$ cells in Fig 7B). Thus, as suggested by the Reviewer, we showed that a second mutation relieved the trapping and transcription repression, without rescuing mRNA decay. As detailed in the text, we argue that R101G displaces Xrn1 from its natural context. Since this has a dominant effect, the R101G displaces the enzyme dead Xrn1 from the decaysome, thus, creating a situation

comparable to Δxrn1. The import capability of DFs is directly correlated with the transcriptional capacity of the cells. We are particularly thankful to Reviewer 2 for suggesting this experiment that substantially improved the paper quality. A more detailed description of the R101G mutation and what we learnt from it is described on pages 10 and 11 (blue paragraphs).

c) We have added four more additional negative controls (random genes we acquired), all of which were unable to grow on plates without Histidine (Table S5). As recommended, we performed both Northern and Western analyses of the GAL4-fusion mRNAs and proteins respectfully (Fig S5F and G). See text in the legend of Fig. S5F and G on page 7 of the Supplemental information, highlighted in blue (due to severe space problem, we moved this text to the supplemental information).

2)

a) Recently, transcriptional and mRNA decay responses to environmental cues has been reported. This whole genome analysis found that families of genes, whose transcription is co-regulated, also are degraded in a coordinated fashion, maybe by a common mechanism (Shalem et al., 2008). This work is now cited in the Discussion of the revised manuscript (see page 20, blue sentences).

b) As an alternative to a), Reviewer 2 suggested that we provide initial insight into the mechanism of transcriptional control by decay factors. Initial GRO data suggested a role in elongation (Fig 6A). In response to this comment, we decided to analyze the possible role of Xrn1 in elongation further. This research is discussed in a new chapter entitled "*Decay factors affect transcription elongation*" and its results are shown in Fig. 6 and S6.
All in all, we suggest that DFs have a role in elongation (this does not exclude a role in initiation). Another mechanistic insight is provided by the capacity of the enzyme dead Dcp2, Dcp2-4, to stimulate transcription in the tethering assay, much like the WT Dcp2 (Fig. 5E). This issue is discussed on page 24, blue sentences.

3) The sentence regarding the phenotype of xrn1208A during meiosis was removed due to lack of space. The reference that should have been there is Solinger et al., 1999. This reference is cited in the manuscript.

Reviewer 3

We would like to thank Reviewer 3 for his/her review and comments that helped us improve our manuscript. In response to his/her comments, we have performed the following experiments and clarifications in the text:

Major points:

1. The issue of direct vs indirect effect is important and we would like to elaborate on this. We argue that DFs play a direct role in transcription based on the following observations, many of which are new and included for the first time in this revised MS:

   (I) DFs are imported to the nucleus in a regulated manner (Fig. 4 and S4).

   (II) DFs bind chromatin (Fig. 5 and S5).

   (III) Binding of Xrn1 to *GAL1* chromatin increases upon transcriptional stimulation by galactose (Fig. 5C). Binding of Dcp2 to chromatin is compromised when transcription is compromised due to the D208A mutation in *XRN1* (Fig. S5D).

   (IV) Binding of DFs to chromatin is direct, not via RNA (Fig. S5C).

   (V) Although mRNA decay in Δ*xrn1* and *xrn1*^{D208A} cells is comparably defective (Figs. 2B, S2F), their transcription capacity is different (Figs. 2A, S2E-F). This argues against an effect through mRNA stability.

   (VI) There is a direct correlation between Xrn1 capacity to mediate mRNA decay and transcription. The greater the effect of Xrn1 disruption on mRNA stabilization, the greater its effect on transcription (Fig. 7A). This can also be deduced from the constant RA that does not significantly change in response to change in HL as shown in Figs. 1A and C.

   (VII) DFs are capable of stimulating transcription when artificially tethered to promoters (both reporter and the natural *GAL10* promoters) (Fig 5E-F). Gal4-BD-Dcp2-4p, which is forced to be tethered to the promoter by the Gal4-BD and its NLS, is as effective as Gal4-BD-Dcp2p in stimulating transcription, indicating that transcription stimulation is not dependent on decapping-dependent decay.

   (VIII) Numerous genetic and physical interactions between DFs and factors that participate in transcription have been documented (Table S3).

   (IX) A direct correlation between import of DFs and transcription. Compare the transcriptional capacity of *xrn1*^{D208A} cells, which poorly import DFs, with that of Δ*xrn1* cells, which import DFs efficiently (Fig. 4B and S4G and Fig. 1D vs S1C, and S3G, 2A-B, S2E, 7B). Perhaps the most striking linkage between import and transcription is provided by introduction of R101G mutation into Xrn1^{D208A} mutant form (Fig. 4B and 7B). See text on pages 10 and 11, blue sentences.

   Each observation by itself is not sufficient to make a case. However, the combination of all these observations, many of which were made in response to the reviewers' comments, now makes a strong case that DFs directly affect transcription.

2. We thank Reviewer 3 for challenging our FISH analyses. This discussion helped us to better communicate these experiments with future readers. First, luckily for us, it has been recently shown that splicing occurs co-transcriptionally in yeast (Churchman and Weissman, 2011). We note that, regardless of Churchman and Weissman publication, we always detected not more than one spot in the nucleus. If splicing had occurred at a location different from the transcription site, we would have detected at least 2 spots inside the nucleus. We should emphasize that this very specific FISH method was scrutinized by a number of referees in the past and many control experiments were performed to unambiguously demonstrate that the single spot is a transcription site (e.g. (Gandhi et al., 2011; Trcek et al., Nat Protoc *7*, 408-419 2012; Trcek et al., Cell *147*, 1484-1497 2011; Zenklusen et al., NSMB 15, 1263-71 2008). In response to this discussion, we referred the readers to both Churchman and Weissman paper and to a review written on this method (Zenklusen and Singer, Methods Enzymol *470*, 641-659 2010). See page 8, blue sentences.
3. Cell to cell variation is observed in any kind of species and it is now a field in cellular and molecular biology. (see, for example, "Single-cell proteomic analysis of S. cerevisiae reveals the architecture of biological noise" Newman et al., Nature 441, 840 [2006]). The figure that we showed is a snapshot. It does not mean that each cell has its own specific expression profile, because in the next snapshot, each individual cell may show a different profile. What we meant to imply in this figure (and failed in doing it properly) is that cell to cell variation suggests that all cells (including those that in this snapshot look normal) are unable to maintain proper mRNA levels. That is to say, the mRNA level fluctuates in the mutant cell more than in WT cells. However, we understand that this conclusion is not strong enough (perhaps labeling mRNAs, using the MS2 system, in live cells and following individual cells by time lapse technology would be the correct method). We therefore removed this figure.
4. We used a standard method to examine shuttling, developed by K. Weise. Using this method, a number of proteins that are seen mainly in the cytoplasm were identified, including Pab1 shown in Fig. 4 and S4 of the revised manuscript. If a protein normally shuttles, preventing its export would result in accumulation in the nucleus. In our assay, cycloheximide does not inhibit the import of the DFs. This indicates that the nuclear accumulation is not of newly synthesized protein molecules but of molecules that existed in the cytoplasm prior the heat inactivation. This is a hallmark of a shuttling protein (see see Brune et al., RNA *11*, 517-531 2005). Protein that is actively and constantly imported (as this assay shows), and exported (excluding a protein that finds itself in the nucleus can be done only by export) is by definition a shuttling protein. In the revised MS we show that this import is does not occur by default, since import of various DFs is dependent on some features of Xrn1 (see Fig. 4B-C and S4G) and it is **specific**, since different xrn1 mutants differentially affected the import of Dcp2, but <u>not</u> Pab1. We believe that now, with all the additional data presented in Fig. 4B-D, this conclusion is solid.

As to the paper by Johnson: the observation that only Xrn1 with a strong NLS can complement the rat1-1 mutant is consistent with our suggestion that, normally, Xrn1 is imported as a complex and that this complex functions within a certain context in the nucleus (i.e. Xrn1 is not "available" to do jobs that it is not designed to perform). It is quite possible, for instance, that native Xrn1 is engaged in protein complexes that do not allow it to complement *rat1-1*, or that the exonuclease activity of *XRN1* is inhibited while in the nucleus, and the exonuclease activity is resumed only in the cytoplasm. The Xrn1-NLS may bypass these two possibilities and therefore can complement *rat1-1* [one should note that this is a very strong SV40 NLS]. Indeed, we propose that $Xrn1^{R101G}$ is abnormally imported (its import is defective but a small portion of it somehow manages to enter the nucleus) - outside the normal context. This is why despite its import, transcription in these cells is like that in Δxrn1 cells (see Fig. 7B). There are many examples in the literature for activities that are context dependent. For example, we showed that Rpb4/7 could interact with the mRNA in the nucleus only in the context of RNA polymerase II. This is despite the presence of vast excess (10 to 50 fold) of Rpb4/7 in the nucleus that is not associated with Pol II. Only the small portion of Rpb4/7 that is bound to Pol II manages to interact with the transcript (Goler-Baron et al., G&D *22*, 2022-7, 2008; Harel-Sharvit et al., Cell *143*, 552-563 2010). We (Bregman et al., Cell 2011) and Rob Singer (Trcek et al., Cell 2011) have recently shown that promoters can recruit some regulatory factors that interact with the emerging transcript co-transcriptionally and affect its cytoplasmic decay. Although these factors are found all over the nucleus, they can bind RNA only in the context of specific promoters.

5. In response to this comment, we included in the legend to Fig. 5A the relative level of amplicon 115 that was taken as 100%. The signal of this amplicon relative to that of "No-TAP" (i.e., the signal obtained when we used extract from isogenic strain that contained no tag) was 7.1±2.6 fold. The increase in signal over the ORF relative to the promoter is consistent with a role we show in the revised MS for Xrn1 in elongation, more than initiation.
6. Again, the difference in the two cases lies in the context. The context of Gal4p-BD-Dcp2-4 and the natural Dcp2 is different. We suggest that, due to the strong artificial NLS and the strong DNA-binding domain of Gal4, which are missing in Dcp2-4p, Gal4p-BD-Dcp2-4p is placed outside of its normal context (remember that these cells contain normal Dcp2 that probably outcompetes Gal4-BD-Dcp2-4 for assembly with the decaysome) and finds its way to the transcription apparatus independently of the mRNA decay process. We would like to thank Reviewer 3 for this question, which helped us to clarify this issue in the text. See a blue paragraph that starts on page 12 and ends on page 13.
7. We agree with Reviewer 3 that in Δ*xrn1* cells, mRNA level expressed in the absence of an activator (the "empty vector") is higher than in WT cells. This is consistent with the mRNA higher stability (in this artificial case, the feedback between mRNA decay and transcription does not seem to occur).

8. In the revised manuscript, we added important results (shown in Fig. 4B and 7B) of an experiment suggested by Reviewer 2, which helped us consolidate our statement. We introduced a second mutation (R101G) into Xrn1^{D208A}. This second mutation compromises Xrn1 RNA- binding capacity. Obviously, this mutation does not rescue mRNA decay. Strikingly, this mutation recovered Dcp2 import (Fig 4C) and improved the ability of the cells to transcribe GAL genes, (compare transcriptional performance of *xrn1*^{D208A} cells with that of *xrn1*^{D208A,R101G} cells in Fig 7B). Thus, we showed that a second mutation relieved trapping and transcription repression, without rescuing mRNA decay. As detailed in the text, we argue that R101G displaces Xrn1 from its natural context. Since this has a dominant effect, the R101G displaces the enzyme dead Xrn1 from the decaysome, thus, creating a situation comparable to Δ*xrn1*. The import capability of DFs is directly correlated with the transcriptional capacity of the cells.
   A more detailed description of R101G mutation and what we learnt from it is described on pages 10 and 11 (blue paragraphs).
   The two independent approaches whose results are depicted in Fig 7, combined with the number of observation showing a direct role for DFs in transcription (see item #1) now strongly support the notion that the capacity of Xrn1p to bind and degrade mRNAs is related to its capacity to stimulate their synthesis. This important issue is now discussed in some detail in the Discussion, taking into consideration the number of new data added to this revised manuscript.

Gene expression is a circular process

Gal Haimovich[1], Sebastien Z. Causse[2], Daniel Medina[3],Gonzalo Millán-Zambrano[4], Oren Barkai[1], José E. Pérez-Ortín[3], Sebastián Chávez[4], Xavier Darzacq[2] and Mordechai Choder[1*]

[1]Department of Molecular Microbiology, Faculty of Medicine, Technion-Israel Institute of Technology, Bat-Galim,31096 Haifa, Israel. [2]Functional Imaging of Transcription, Ecole Normale Supérieure, CNRS, IBENS, 46 rue d'Ulm 75230 Paris cedex 05. [3]Departamento de Bioquímica y Biología Molecular, Facultad de Biológicas and ERI Biotecmed, Universitat de València, Dr Moliner 50, E-46100 Burjassot, Valencia, Spain. [4]Departamento de Genética, Facultad de Biología, Universidad de Sevilla, Avda. Reina Mercedes 6, E-41012 Sevilla, Spain.

* Corresponding author

Tel: (972) 4 829-5423

Fax: (972) 4 829-5225

E-mail: choder@technion.ac.il

Summary

Maintaining the proper level of mRNAs is a key aspect in the regulation of gene expression. The balance between mRNA synthesis and decay determines these levels. Using a whole-genome analysis, we demonstrate that most yeast mRNAs are degraded by the 5' to 3' pathway (the "decaysome"), as proposed previously. Unexpectedly, the level of these mRNAs is highly robust to perturbations in this major pathway, as defects in various decaysome components lead to down-regulation of transcription. Moreover, these components shuttle between the cytoplasm and the nucleus, in a manner dependent on proper mRNA degradation; in the nucleus, they associate with chromatin and directly stimulate transcription initiation and elongation. Hence, the major decaysome has a dual role in maintaining mRNA levels. Significantly, proper import of some decaysome components seems to play a key role in coupling the two functions. Gene expression process is therefore circular, whereby the hitherto first and last stages are interconnected.

Introduction

Gene expression is traditionally divided into several stages, including mRNA synthesis and processing, export (in eukaryotes), translation and decay. Yet, gene expression can be viewed as a single system in which all stages are mechanistically coupled (Komili and Silver, 2008) and probably coordinated by master regulators (Harel-Sharvit et al., 2010). An essential and well-controlled component of this system is the cytoplasmic mRNA decay pathway, considered to represent the end-point of the mRNA life. Following shortening of the mRNA poly(A) tail by the Ccr4p-Notp and Pan2p/3p complexes, the eukaryotic mRNA can then be degraded by two pathways: from 3' to 5' by the exosome or from 5' to 3' by the Xrn1p exonuclease (Garneau et al., 2007). The latter pathway involves prior removal of the 5'-cap by the Dcp2p enzyme assisted and regulated by Dcp1p, Pat1p, Dhh1p, Edc1/2/3p and the Lsm1-7p complex. In *Saccharomyces cerevisiae*, it is proposed to be the major degradation pathway (Anderson and Parker, 1998; Coller and Parker, 2004), although this issue is still debateable (He et al., 2003). Conventional wisdom holds that, following the completion of the degradation of a certain mRNA, the mRNA decay factors (DFs) re-enter the decay process of yet another mRNA in the cytoplasm. Other options have not been systematically examined.

Results

Steady state mRNA levels are highly robust to perturbations in mRNA decay

The rates of mRNA synthesis and decay determine the steady state level of mRNA (also referred herein as mRNA abundance –RA). Accordingly, a defect in mRNA decay is expected to result in an increase in mRNA levels. As expected, elevated levels of *EDC1* and *RPS28B* mRNAs were observed in cells lacking various genes encoding DFs (Figs. 1A and S1A), as previously reported (Badis et al., 2004; Muhlrad and Parker, 2005). Surprisingly, the levels of various other mRNAs did not increase in strains lacking these DFs (Figs. 1A and S1A), despite their increased stabilities (Fig. 1B). Some levels even decreased in the mutants (Fig. 1A and S1A). These results prompted us to pursue a whole genome analyses. To this end, we determined both the RA and half lives (HL) of most yeast mRNAs, using a thiolutin shut-off protocol (Pelechano et al., 2008). As shown in Fig. 1C, Xrn1p - the only known cytoplasmic 5' to 3' exonuclease - is involved in the degradation of most, if not all mRNAs since most mRNAs were stabilized by deletion of *XRN1* (Fig. 1C and Table S1). Thus, as proposed previously (Anderson and Parker, 1998; Coller and Parker, 2004), Xrn1p-mediated decay is a major cytoplasmic pathway for mRNA degradation in yeast. Second, consistent with the Northern analysis, most spots scattered around or below the ratio 1. Importantly, no correlation was found between the effect of *XRN1* deletion on mRNA half-lives and its effect on mRNA level (Fig. 1C). This suggests that changes of mRNA HL are compensated by inverse changes in mRNA synthesis. A list of a few hundred mRNAs whose stability was severely affected by *XRN1*deletion is shown in Table S1. The levels of these mRNAs were little perturbed. These results are consistent with

previous data demonstrating that the levels of most mRNAs in Δ*xrn1* and Δ*dcp1*cells are not higher than those in wild-type (WT) cells (He et al., 2003; Muhlrad and Parker, 1999). We used the Northern analysis data of RA (Fig. 1A and S1A), and mRNA half lives (HL) (Fig. 1B) to calculate the transcription rate (TR) of each mRNA in stains harbouring deletion in *XRN1*, *DHH1* or *PAT1*, relative to WT. These calculations, based on a single mRNA analysis, indicate that transcription is down-regulated when the decay process is defective and that this is not specific to a certain DF (Table S2). Note that the TR of *EDC1* and *RPS28B* mRNA is also reduced despite an increase in its apparent level. We therefore hypothesized that in addition to their role in mRNA decay, the DFs have the capacity to enhance transcription, either directly or indirectly. This notion is supported by prior studies demonstrating numerous physical and genetic interactions of various DFs with factors that are involved in the nuclear stages of gene expression (Table S3 and Fig. S1B).

Disruption of Xrn1p affects transcription of most genes

To determine transcription efficiency on the whole genome level, we performed genomic run-on (GRO) experiments. This allowed us to measure transcription rates (TR) and mRNA abundance (RA) directly (Garcia-Martinez et al., 2004; Pelechano and Perez-Ortin, 2010). Consistent with our results obtained by single gene analysis (Table S2), TR of most genes expressed in Δ*xrn1*cells decreased relative to WT (median of 4.7 fold) (Fig. 1D).

We next compared the TR obtained in these Δ*xrn1* cells to the TR in cells carrying an enzyme dead Xrn1p whose aspartic acid located at the active site was replaced with alanine ($Xrn1^{D208A}p$) (Chang et al., 2011; Jinek et al., 2011). $Xrn1^{D208A}p$

is expressed at a similar level to the WT protein, and binds uncapped mRNA (Solinger et al., 1999) as efficiently as Xrn1p, but does not degrade it (Solinger et al., 1999). Interestingly, *xrn1*^{D208A} cells were more defective than the Δ*xrn1*cells in transcription (median of 8.5 fold), as better illustrated in the histogram in Fig. S1D. TR values are listed in Table S4. This poorer transcription is not due to decreased proliferation rate of *xrn1*^{D208A} relative to Δ*xrn1*cells or a difference in P-body (PB) formation (Fig. S1E-F).

Transcriptional induction is dependent on mRNA decay factors

Next, we investigated *de novo* mRNA synthesis and mRNA decay in response to various environmental signals in WT, Δ*xrn1*, and *xrn1*^{D208A}. First, we monitored *de novo* mRNA synthesis in response to galactose that induces transcription of *GAL* genes. We then shifted the cultures to glucose medium to repress their transcription in order to monitor the decay of *GAL* mRNAs (Lohr et al., 1995). As expected, in WT cells, galactose stimulation rapidly induced transcription of *GAL* genes (Fig. 2A), and glucose addition led to rapid transcriptional repression, which was followed by rapid mRNA degradation (Fig. 2B). Consistent with the GRO results, accumulation of mRNA in the *xrn1*^{D208A} strain lagged behind the WT and was slow, indicating a clear defect in transcriptional induction (Fig. 2A). Although deletion of *XRN1* led to stabilization of *GAL* mRNAs (Fig. 2B), mRNA accumulation in the Δ*xrn1* strain was comparable to that in the WT cells (Fig. 2A). The half-life of *GAL10* mRNA in WT cells proliferated in galactose media is 20 min (Munchel et al., 2011)- the time frame of the experiment; therefore, we would expect to detect more mRNA in *Δxrn1* cells, if transcription was not affected. The comparable accumulation of the *GAL10* mRNA in the Δ*xrn1* and WT cells suggests, therefore, a defect in transcription in this mutant as well. This conclusion

is in accord with the poor performance of Δ*xrn1* cell extract in the run-on assay (Fig. 1D). Significantly, since the effect of D208A mutation on mRNA stability was identical to that of *XRN1* deletion (Fig. 2B), we concluded that the different accumulation of mRNAs in these mutants (shown in Fig. 2A) is solely due to a difference in their transcriptional capacity. Note that the different transcription rates cannot be attributed to the proliferation rate (Fig. S1E) (Solinger et al., 1999) or to PB formation (Fig. S1F).

We also assessed transcriptional induction and mRNA decay of heat shock (HS) genes in response to HS, and non-HS genes during recovery from HS. We compared WT to *xrn1* mutant strains, discussed above. We also examined Δ*dcp2* and *dcp2-4* strains. The *dcp2-4* mutant carries a single mutation, E153Q, rendering the product enzyme dead (Dunckley and Parker, 1999). As shown in Figs. S2C and S2A, C and E, transcription of these genes was efficiently induced in WT, yet it was defective in the *xrn1* and *dcp2* mutant strains. The transcriptional defect was, again, more pronounced in both enzyme-dead strains compared to their respective deletion strains. The stability of all these mRNAs was increased in the mutant strains. Significantly, stabilities of these mRNAs were comparable in the deletion and enzyme-dead strains (Figs. 2 and S2).

Interestingly, both transcription and decay of a non-coding RNA (ncRNA), *SUT508*/*TIR1axut* (which is partially anti-sense to the gene *TIR1*) was found to be dependent on functional Dcp2p (Fig.S2G-H). Moreover, *SUT508* RNA stability was dependent on *PAT1* and *DHH1* (Fig. S2I), yet its steady state was not (time 0 in the same panel). These results suggest that various DFs are also involved in transcription and decay of Pol II transcribed ncRNAs.

Collectively, these results suggest that the presence or absence of Xrn1p and Dcp2p, regardless of their enzymatic activities, affects transcription. The reason why

xrn1^{D208A} cells are more defective in transcription than the other *xrn1* mutants is discussed later.

Xrn1p affects Pol II occupancy on TEF4 gene.

In order to better understand the transcriptional defect characterizing *xrn1* mutant cells, we employed fluorescent *in situ* hybridization (FISH) analysis designed to detect single mRNA molecules and to identify specific nuclear transcription sites (TSs) (Femino et al., 1998; Zenklusen et al., 2008) (Figs. 3 and S3A and B). This method has been reviewed in (Zenklusen and Singer, 2010). We focused on *TEF4* as it contains a large intron that helped us identify TSs, which can be recognized by both exonic and intronic probes. *TEF4* intron is processed into *snR38*, a snRNA which resides in the nucleolus. The nucleolar signal was used as a positive control (Fig. 3A and B). Only mature, intronless, *TEF4* mRNAs were detected in the cytoplasm. Reassuringly, the average number of single *TEF4* mRNA molecules detected in the cytoplasm of a single WT cell is consistent with previously published results (Velculescu et al., 1997) and is comparable to those detected in *xrn1*^{D208A} and Δ*xrn1* cells (Fig. S3C). The similar values in these strains are consistent with the similar steady state levels of *TEF4* mRNA obtained by Northern analysis (Fig. S3D). A single TS was detected in these haploid nuclei, using either the double probes (Fig. 3B) or three dimensional (3D) reconstructions of cells labelled with the ORF probes (Fig. 3C, Movies S1 to S3). This indicates that splicing of *TEF4* occurs co-transcriptionally, consistent with previous results (Churchman and Weissman, 2011) or at least close enough to the TS to be indistinguishable by our FISH analysis. Most WT and Δ*xrn1* cells (88%) contained a TS, whereas only 66% of the *xrn1*^{D208A} cells contained a TS ($p=2.6x10^{-8}$) (Fig. 3D-G,

S3E-G and Movie S4). This is consistent with our Northern and GRO analyses showing that the transcriptional defect of *xrn1*^{D208A} cells is more severe than that of WT or Δ*xrn1* cells (Figs. 1C, 2, S1C-D and S2, Table S4).

Moreover, WT cells contained TSs with more than one transcript (equivalent to multiple elongating Pol II occupancy) (Fig. 3D and E) that is indicative of frequent transcription initiation or re-initiation events (Zenklusen et al., 2008). In contrast, Δ*xrn1* and *xrn1*^{D208A} cells contained TSs with only one transcript (Fig. 3F-G and S3E-G) suggesting that Xrn1p is required for either transcription initiation, elongation or both. Note that nuclear export of the *TEF4* mRNA in both *xrn1* mutant strains was normal as no nuclear accumulation could be observed by FISH analysis outside the TS context (Figs. 3B and C, Movies S1 to S4 and results not shown).

Various mRNA decay factors shuttle between the cytoplasm and the nucleus in a manner dependent on proper mRNA decay

The studied DFs are detected by and large in the cytoplasm (e.g.(Teixeira and Parker, 2007). We next determined whether they also reside in the nucleus, utilizing the temperature sensitive *xpo1-1*, *mex67-5* strain to assay the nucleocytoplasmic shuttling activity of the DFs, and using Pab1p as a positive control (Brune et al., 2005). Similarly to Pab1p-GFP, all tested DFs accumulated in the nucleus upon heat inactivation of the exportins Xpo1-1p and Mex67-5p. Nuclear accumulation was insensitive to translation inhibition by cycloheximide (CHX), added concomitantly with the heat inactivation (Figs. 4A and S4A). Translation independent import indicates that the same protein molecules, which had been present in the cytoplasm prior the heat inactivation, entered the nucleus. It is worth noting that nuclear accumulation of Pat1p and Dhh1p in a Δ*lsm1*

strain was reported previously (Teixeira and Parker, 2007), suggesting that they are exported in complex with Lsm1p.

These observations and ours led us to conclude that all the examined DFs normally shuttle between the two compartments. We suspect that these DFs are usually visualized in the cytoplasm because their export rate exceeds their import rate. Interestingly, the equilibrium between export and import kinetics could be altered in response to environmental cues such as starvation (Fig. S4B-E and G) or HS (Fig S4F). Furthermore, nuclear accumulation of some of the examined DFs could be detected in several WT strains under optimal conditions (Fig. S4B-C).

In order to assess whether nuclear import of DFs is dependent on proper mRNA decay, the same shuttling assay was performed using various *XRN1* mutants. Import of Xrn1^{D208A}p-GFP was severely impaired (Fig. 4B; compare Xrn1 and Xrn1^{D208A}). Xrn1^{D208A}p binds mRNAs without degrading it (Solinger et al., 1999). Combination of these two features might block its import. To test this hypothesis, we introduced a second mutation to disrupt Xrn1^{D208A}p RNA binding activity. Two such mutations were considered, R101G and H41D; both disrupt the capacity of Xrn1p active site to bind decapped RNA (Jinek et al., 2011; Page et al., 1998), with little effect on proliferation rate (Fig S1E). Remarkably, introducing the R101G mutation into *xrn1*^{D208A} partially restored import capacity, consistent with our hypothesis. However, import of Xrn1^{D208A,R101G}p-GFP was not as efficient as import of the WT Xrn1p-GFP (see p values in Fig. 4B), raising the possibility that the RNA-binding is important, by itself, for efficient import. To examine this possibility, we determined import of Xrn1^{R101G}p-GFP and Xrn1^{H41D}p-GFP. Indeed, import of these proteins was similarly compromised relative to that of Xrn1p-GFP (Fig. 4B, p=0.01 and p=0.02, respectively). Pab1p-GFP

was efficiently and equally imported in all the strains, demonstrating that the import defects of the various *xrn1* mutant cells is not general. In summary, efficient import of Xrn1p requires both its RNA binding capacity, which probably recruits the protein to the correct context, and its capacity to degrade this RNA. Only WT Xrn1p is therefore imported efficiently.

We next assessed the import of Dcp2p-RFP in the various *XRN1* mutant strains (Fig. 4C). Interestingly, Dcp2p-RFP import was severely impaired in $xrn1^{D208A}$ cells (p=0.01), but was efficient in $xrn1^{D208A,R101G}$, $xrn1^{R101G}$, $xrn1^{H41D}$ or Δ*xrn1* cells, as compared to WT cells (Fig. 4B-C). These import features suggest that the combination of binding of Xrn1p to the RNA without degrading it blocks Dcp2p import, as it blocks the import of Xrn1p itself. Furthermore, during starvation, $xrn1^{D208A}$ cells poorly imported various other DFs (Fig. S4G). Collectively, these results suggest that import of DFs does not occur as a default. It seems to require normal Xrn1p that is capable of binding decapped RNA and executing 5' to 3' mRNA decay. As shown below, the import features of Xrn1p are correlated with its capacity to stimulate transcription.

Decay factors associate with chromatin

Next, we examined whether DFs are capable of binding chromatin, using chromatin immunoprecipitation (ChIP) analysis. As shown in Fig. 5A, Xrn1p-TAP associated with chromatin along the *PMA1* gene. Although it is associated with the *PMA1* promoter region, its association increases in the ORF, raising the possibility that Xrn1p is involved in transcription elongation, as shown below. Xrn1p-TAP was also found to be associated with the *TEF4* promoter (Fig. 5B), as well as with other

promoters and ORFs (Fig. S5A), but not with rDNA (Fig. 5B). As expected, association of Xrn1p-TAP with *GAL1* ORF increased upon transcriptional induction of *GAL1* by its inducer, galactose (Fig. 5C). Several other tagged factors, except for Dcp1p, associated with *PMA1* and *TEF4* promoters (Fig. 5D and S5B), as well as with other genes (results not shown). The chromatin association of Xrn1p-TAP and Dcp2p-TAP was independent of RNA, since RNase treatment did not decrease the ChIP signal (Fig S5C). We suspect that the slight increase in the Xrn1p-TAP ChIP signal after RNase treatment is a result of better accessibility of the protein A tag to the IgG beads. Our localization analysis shows that the import of Dcp2p is inhibited in *xrn1*^{D208A} cells (Fig 4C). We therefore tested whether the ChIP signal of Dcp2p-TAP is affected by this mutation. Consistently, less Dcp2p-TAP was found associated with chromatin in *xrn1*^{D208A} cells compared to WT cells (Fig.S5D). Collectively, our ChIP results are consistent with a direct role of these DFs in transcription.

Decay factors activate transcription when tethered to promoters

Our results so far are consistent with a direct role for DFs in transcription. To further corroborate this novel role, we examined whether they are capable of stimulating transcription when artificially recruited to reporter promoters (Titz et al., 2006). We fused the DFs to the Gal4p-DNA binding domain (Gal4p-BD) and analyzed transcriptional activation of the reporter genes, P_{GAL1}-*HIS3* and P_{GAL7}-*lacZ* as well as the natural *GAL10* gene.

Transcription of these genes was stimulated by recruitment of some of the DFs to their promoters (Figs. 5E-F and S5E). Importantly, Gal4p-BD-Dcp2-4p, a mutant

lacking decapping activity, activated transcription similarly to Gal4p-BD-Dcp2p (Figs. 5E-F and S5E). This is in contrast with the defective capacity of *dcp2-4* cells to mediate transcription (Fig. 2C and S2C). We argue that, due to the strong artificial NLS and the strong DNA-binding domain of Gal4, which are missing in Dcp2-4p, Gal4p-BD-Dcp2-4p is placed outside of its normal context and finds its way to the transcription apparatus independently of the mRNA decay process. We conclude that the decapping activity of Dcp2p *per se* is not necessary for its capacity to stimulate transcription. In the natural context, the decapping is necessary to enable 5' to 3' decay that, in turn, is required for transcription (see below).

Although we showed that many DFs shuttle between the cytoplasm and nucleus as well as associate with chromatin (Figs. 4, 5, S4 and S5), not all were able to activate transcription. This may either reflect a true biological role, or may be due to differences in expression levels of the fusion genes, or the effect of the Gal4p-BD moiety (see legend to Fig. S5F-G).

Importantly, in the absence of active Xrn1p, Gal4p-BD-Dcp2p (Fig. 5G) was unable to induce transcription, indicating that Xrn1p is required for transcriptional activation by Dcp2p. Taken together, these results, combined with the role assigned to these factors in transcription discussed earlier, argue against a trivial effect of DFs in this tethering assay.

Summarily, our combined results so far directly implicate some DFs in transcription. It is quite possible that those DFs, which apparently cannot function as activators but are required for transcription (e.g., Xrn1p), enable the activators (e.g. Dcp2p) to function in transcription.

Decay factors affect transcription elongation

Unexpectedly, our GRO analysis revealed a direct correlation between the negative impact of Xrn1p disruption on transcription and the ORF length (Fig 6A), consistent with a role in transcription elongation (Morillo-Huesca et al., 2006; Rodriguez-Gil et al., 2010). To examine this possibility further, we first used our previously developed assay to examine the distribution of either Pol II molecules by means of ChIP, or the distribution of transcriptionally active Pol II by means of GRO (Rodriguez-Gil et al., 2010). We used a membrane containing 5' and 3' probes of 384 ORFs that enabled us to determine how Pol II molecules (Rpb3p ChIP) or Pol II activity (run-on) are distributed in the 3' portions relative to the 5' portions of these ORFs. Statistical analysis of the ChIP data revealed a bias in the 3'/5' ratio of Pol II occupancy in *xrn1* mutants relative to WT ($p \leq 2.75e^{-16}$) (Fig. 6B blue columns). This indicates that, in *xrn1* mutant cells, Pol II molecules accumulate more in the 3' portions of the examined ORFs than in WT. Remarkably, these surplus Pol II molecules were transcriptionally inactive, as the 3'/5' ratios of the run-on signals of the mutants were comparable to that of the WT (Fig. 6B, red columns). Note that when Pol II encounters nucleosome or other obstacles, it reverses its direction and back-tracks, leaving the transcript 3'-end miss-aligned with the active site and therefore cannot polymerase any further (Cheung and Cramer, 2011). Accumulation of inactive Pol II molecules is a hallmark of backtracking Pol II (Pelechano et al., 2009; Perez-Ortin et al., 2011; Rodriguez-Gil et al., 2010). Xrn1p might improve Pol II processivity by preventing backtracking or stimulating resumption of elongation. This effect is more apparent in the last stages of transcription elongation, as was observed previously when *SSD1*, *CCR4*, or *BUR2* were deleted (Rodriguez-Gil et al., 2010).

We next similarly examined Pol II occupancy and its activity along the *GAL1* gene after induction by galactose. Consistent with the whole genome data shown in Fig. 6B, Pol II occupancy increased by disruption of Xrn1p (Fig. 6C), whereas its *in vitro* activity did not. Specifically, the ratio between run-on signals in the mutant vs WT was maintained in the 5' (arbitrarily defined as 1), middle, and 3' portion of the gene (Fig S6A). Phosphorylation of Pol II CTD heptad repeat at Ser-2 position is one hallmark of elongating Pol II (Bataille et al., 2012; Meinhart et al., 2005). Consistent with a role for Xrn1p in elongation, Ser-2 was hypo-phosphorylated in *xrn1* mutants compared to WT cells (Fig 6C).

TFIIS resolves hindrance caused by back-tracking by inducing internal cleavage of the nascent RNA within the back-tracked Pol II, realigning the 3' end with the active site (Cheung and Cramer, 2011) and references therein). This increases Pol II processivity as it traverses through nucleosomes or other obstacles (Churchman and Weissman, 2011). We used our tethering assay to ask whether the tethered DFs stimulate transcription whose elongation is dependent on TFIIS. Two classes of responses were observed. As expected (see (Mason and Struhl, 2005)), deletion of *DST1*, encoding the yeast TFIIS, led to a decrease in Gal4p-BD-Dcp2p and Gal4p-BD-Dcp2-4p driven transcription, much like its effect on our positive control Gal4p-BD-Rpb3p (Fig. S6B). Interestingly, transcription that was driven by Gal4p-BD-Ccr4p, Gal4p-BD-Dhh1p and Gal4p-BD-Pat1p was slightly increased in Δ*dst1* cells (Fig S6B). These differences indicate that the nature of the Gal4p-BD fusion protein can affect the mechanism of transcription elongation. We suggest that, when recruited to promoters, Ccr4, Dhh1 and Pat1 affect both transcription initiation (which maybe repressed by

TFIIS; see (Kim et al., 2007)) and transcription elongation in a pathway that is distinct from TFIIS.

The drug 6-azauracil (6-AU) depletes NTPs thereby reducing both the elongation rate and Pol II processivity, and this processivity defect is aggravated by mutations in elongation factors (Mason and Struhl, 2005). Therefore, 6-AU sensitivity is often indicative of a defect in transcription elongation (e.g. (Fish and Kane, 2002; Hartzog et al., 1998; Malagon et al., 2006; Mason and Struhl, 2005)). Indeed, some decay mutants were hypersensitive to 6-AU (Fig S6C), reinforcing our conclusion that they are involved in transcription elongation.

Taken together, Pol II occupancy, Ser-2 phosphorylation status and run-on experiments indicate that defects in Xrn1p lead to accumulation of inactive hypo-phosphorylated Pol II, scattered mainly in the 3' portions of transcribed genes. Interestingly, *PAT1*, *LSM1* and *CCR4* are synthetically lethal with *DST1* (Table S3), suggesting that transcription elongation requires at least one of the pathways, either the TFIIS-dependent or the alternative pathway - mediated by some DFs. Thus, Xrn1p probably affects modifications that occur late in transcription elongation that prevent back-tracking. This mechanism becomes critical upon depleting NTPs by 6-AU.

Transcription is linked to mRNA decay

Our finding that transcription is severely compromised upon disruption of Xrn1 enzymatic activity suggests that the novel role of Xrn1p in transcription is mechanistically linked to its role as RNA exonuclease. If the two functions are indeed linked, one expects that a defect in one function would affect the other. To examine this possibility, we first analysed the GRO and half lives (HL) data. Specifically, we

arbitrarily (in an unbiased manner) classified the mRNAs according to the effect of Xrn1p disruption on their decay rate (DR). Remarkably, we found a direct correlation between the capacity of the strains to degrade mRNAs and to synthesize them (Fig. 7A). This conclusion is also implied by the data in Fig. 1C. Note that *xrn1*^{D208A} cells are more defective in transcription than Δ*xrn1* cells. Thus, for any given strain, the more mRNA decay is dependent on Xrn1p, the more its synthesis is affected by disrupting Xrn1p activity. This suggests that the capacity of Xrn1p to degrade mRNAs is related to its capacity to stimulate their synthesis.

Second, if the function of Xrn1p in transcription is linked to its function in mRNA decay, it might be possible to uncouple these two roles. We examined whether mutating either Xrn1p RNA-binding capacity (R101G), its enzymatic activity (D208A) or both activities (D208A, R101G) can uncouple the two functions by monitoring transcriptional induction and decay rates. Plasmid-borne Xrn1p-GFP and its mutant derivatives were expressed in a strain lacking the chromosomal *XRN1* (see Fig. 4B). Cells were stimulated with galactose to induce transcription of *GAL* genes, and then shifted to glucose medium to repress their transcription. As expected, in WT cells, galactose stimulation induced transcription of *GAL* genes (Fig. 7B), and glucose addition led to rapid transcriptional repression, which was followed by rapid mRNA degradation (Fig. 7C). The *xrn1*^{D208A} cells displayed a substantial decrease in transcriptional induction (Fig. 7B), consistent with the results shown in Fig. 2B. However, their response to glucose was unexpected; mRNA accumulation continued for > 5 min after glucose addition (Fig. 7C). It should be noted that *xrn1*^{D208A} strain is capable of sensing and responding to glucose like its Δ*xrn1* counterpart, as it begins inducing transcription of *HXT1* concurrently with Δ*xrn1* strain (results not shown).

Continued mRNA accumulation is consistent with slow elongation rate; thus, the Pol II that had started transcription before glucose addition slowly reaches the polyadenylation site, replenishing new (stable) mRNAs even after glucose was added (see (Mason and Struhl, 2005). Nevertheless, slow repression of transcription initiation cannot be excluded. It should be noticed that continued synthesis was not observed in the strain harbouring a chromosomal D208A mutation that was used in Fig. 2B. We suspect that the different response to glucose exhibited by the *xrn1*^{D208A} strain used here is either due to the GFP tag or expression from a plasmid. In the Δ*xrn1* and *xrn1*^{R101G} strains, accumulation of mRNA upon stimulation with galactose was comparable to that in the WT cells (Fig. 7B), whereas in the presence of glucose, mRNA decay in the two strains was similarly slowed down (Fig. 7C). Since *xrn1*^{R101G} and Δ*xrn1* strains exhibit identical accumulation and decay of *GAL* mRNAs, and because Δ*xrn1* cells are defective in transcription of most genes (Fig. S1C) including *GAL1* under galactose (results not shown), we can conclude that transcription in *xrn1*^{R101G} strain is as defective as it is in Δ*xrn1* strain. These results indicate that Xrn1p RNA-binding activity is important for its capacity to regulate transcription, as it is important for its import (Fig. 4B-C). Remarkably, introducing the R101G mutation into *xrn1*^{D208A} partially recovered the severe transcription defect exhibited by the *xrn1*^{D208A} strain. Consequently, the transcription capacity of the *xrn1*^{D208A,R101G} strain was similar to that of the Δ*xrn1* and *xrn1*^{R101G} strains (Fig. 7B), given that mRNA decay in these three strains was identical (Fig. 7C). Moreover, the slow transcriptional response to glucose was also recovered. Collectively, these results suggest that the D208A mutation *per se* does not disrupt the ability of Xrn1p to function in transcription (since the double mutant harbours the D208A mutation). Rather, D208A affects the interplay between the two opposing roles

of Xrn1p in mRNA decay and transcription, most probably due to its severe effect on import (Fig. 4B-C and S4G). Taken together, the import and transcription capacities of the Xrn1p mutants suggest that Xrn1p has to bind and degrade the mRNA in order to properly stimulate entry of DFs to the nucleus and stimulate transcription. Affecting the mRNA binding and/or degradation capacity of Xrn1p compromise(s) its key role in properly linking transcription with decay.

Collectively, the two independent results, presented in Fig. 7, suggest that the capacity of Xrn1p to degrade mRNAs is related to its capacity to stimulate their synthesis.

Discussion

The appropriate levels of mature mRNAs are maintained by two opposing mechanisms; one is responsible for synthesis in the nucleus and the other for decay in the cytoplasm. Here we show that steady state mRNA levels cannot serve as a reliable assay to examine transcription or decay rates. These levels are robust to perturbations in either transcription (Goler-Baron et al., 2008; Harel-Sharvit et al., 2010) or mRNA decay (this work). Our whole-genome half lives analysis demonstrates that most mRNAs in optimally proliferating yeast cells are degraded by the 5' to 3' exonuclease Xrn1p, as proposed previously (Anderson and Parker, 1998; Coller and Parker, 2004). Nevertheless, disruption of the major decay pathway does not result in elevated steady state levels; in most cases these levels were even decreased (Fig. 1C). Consistently, disruption of this pathway has a minor effect on the proliferation rate of optimally

proliferating cells (Fig. S1D). We propose that this robustness is maintained by the dual role of the "decaysome" in mRNA synthesis and decay.

Coupling of two processes requires that the activity of (a) certain factor(s) in the first process is a prerequisite for its function in the subsequent step. Following this criterion, it was previously found that mRNA decay is coupled to translation, which, in turn, is coupled to mRNA export, maturation, and transcription (reviewed in (Komili and Silver, 2008). Gene expression was therefore considered a linear pathway. Here, we show that factors of the hitherto last stage are shuttling proteins that also stimulate the first stage by physically binding the chromatin. We found that various DFs bind to chromatin (Figs. 5 and S5). Binding of Dcp2p and Xrn1p is not mediated by RNA (Fig. S5C), and is both stimulated by transcription (Fig. 5C) and affected by disrupting the exonucleolytic activity of Xrn1 (Fig. S5D). A whole genome analysis demonstrated that families of genes, whose transcription is co-regulated in response to environmental cues, also are degraded in a coordinated fashion, maybe by a common mechanism (Shalem et al., 2008). The dual role of the decaysome may underlie this coordination.

A number of observations led us to conclude that the novel transcriptional role is not restricted to a limited number of DFs. First, disruption of any DF that we examined downregulated transcription (Figs. 1 and S1 and Table S2). Second, all the examined DFs are shuttling proteins (Figs. 4 and S4). Shuttling of some DFs is affected by disruption of Xrn1p enzymatic activity (Fig. 4B-C and S4G), suggesting that some of them shuttle as a complex. Third, tethering a number of DFs to promoters stimulates transcription. Fourth, a number of DFs associate with chromatin (Figs. 5 and S5). Fifth, Gal4p-BD-Dcp2p transcription is dependent on Xrn1p, or its enzymatic activity (Fig. 5E-G), suggesting cooperation between more than one DF. It is possible that a

significant portion of the 5' to 3' decaysome functions in transcription. The components that play a direct role may be few, whereas others enable (or otherwise regulate) these few to function.

We propose that the mechanism underlying DFs' import plays a key role in the linkage between mRNA synthesis and decay. A positive correlation is found between transcriptional efficiency and the capacity of Xrn1p and other DFs to shuttle as well as to degrade mRNAs. First, binding of Xrn1p to the decapped RNA is required for its efficient import (Fig. 4B) and for efficient transcription (Fig. 7B), suggesting that Xrn1p has to be recruited to the context of the decaysome in order to be imported. Second, cells harbouring *xrn1*^{R101G}, *xrn1*^{H41D}, *xrn1*^{D208A,R101G} or a deletion of *XRN1,* which can import DFs (other than Xrn1p) efficiently, transcribe better than those harbouring *xrn1*^{D208A}, which are defective in importing Xrn1^{D208A}p as well as other DFs (Figs. 4B-C and S4G). D208A, which disrupts the exonucleolytic activity, exerts its adverse effect only if Xrn1p binds the RNA at the 5' end. Thus, only the combination of binding the decapped RNA in the Xrn1p active site without the ability to degrade it blocks import of key DFs (including the Xrn1 mutant form itself). The R101G mutation, which disrupts Xrn1p binding activity, probably displaces Xrn1^{D208A}p from its natural context, creating a situation comparable to complete absence of Xrn1p (Figs. 4B-C and 7B). Third, as shown in Fig. 7A (and can be deduced also from the results in Fig. 1C), the more severe the effect of disrupting Xrn1p function on decay rates is, the more severe it is on transcription. All the above features are consistent with a coupling between the two roles of the decaysome in the two compartments. We propose a model whereby Xrn1p is recruited to the decapped RNA, via its 5'-phosphate binding pocket, and represses premature import of DFs. Only once the RNA has been successfully degraded, Xrn1p

stimulates the import of DFs, which is followed by transcriptional stimulation. Xrn1^{D208A}p represses import constitutively as the RNA is not degraded. This model illustrates the interdependence between mRNA decay, DFs' import and transcription.

Notably, the dependence of Dcp2p on Xrn1p for both its nuclear import (Fig. 4C) and stimulating transcription (Fig. 5E-G) leads us to suggest that DFs are imported to the nucleus and participate in transcription as a complex. Thus, it is quite possible that those DFs that cannot function as transcriptional activators in the tethering assay, but are required for transcription, have a regulatory role.

We have begun unravelling the mechanism by which DFs activate transcription and found that some DFs function in transcription elongation. Deletion of *XRN1* or, even more so, disruption of its exonuclease activity, leads to accumulation of hypophosphorylated transcriptionally incompetent Pol II at the 3' end of ORFs. Notably, deletion of some elongation factors, such as TFIIS, results in accumulation of Pol II in 5' portions of ORFs whereas others in 3' portions (Churchman and Weissman, 2011; Kruk et al., 2011; Mason and Struhl, 2005; Rodriguez-Gil et al., 2010). A main function of TFIIS is to help Pol II to traverse through the nucleosomal templates, and its deletion leads to accumulation of Pol II within the first four nucleosomes (Churchman and Weissman, 2011). The mechanism underlying the second group of elongation factors, among them are Ssd1p, Bur2p (Rodriguez-Gil et al., 2010) and Ccr4p (Kruk et al., 2011; Rodriguez-Gil et al., 2010), is relatively little understood. As shown in Fig. 6, Xrn1p belongs to the second, less studied, group. Interestingly, we and other investigators have found that Ccr4p-Not complex also belongs to the second group (Kruk et al., 2011; Rodriguez-Gil et al., 2010), raising the possibility that Xrn1 and Ccr4-Not play a role in a common proteinacious context. Deleting *DST1* (TFIIS) did not

compromise the capacity of Pat1p, Ccr4p and Dhh1p to stimulate transcription in the tethering assay (Fig. S6B). Interestingly, Dcp2p and Dcp2-4p capacity to promote transcription was impaired by deleting *DST1* (Fig. S6B), suggesting that not all DFs function alike. Our data are consistent with a model whereby Xrn1p prevents Pol II from backtracking, thereby stimulating elongation in a manner independent of TFIIS. In recent years it has become clear that recruiting Pol II to transcription start sites is insufficient to promote transcription and that post-initiation stages play key roles. The roles of DFs in elongation add an additional level of complexity to the regulations that occur after transcription begins.

The decaysome may affect transcription by degrading regulatory RNAs (e.g., ncRNAs) (Geisler et al., 2012; van Dijk et al., 2011). However, our current data are more consistent with a degradation-independent mechanism. First, DFs bind chromatin. This binding is direct, and not mediated by RNA (Fig. S5C), is stimulated by transcription (Fig. 5C) and is affected by disrupting the exonucleolytic activity of Xrn1 (Fig. S5D). Second, DFs bind promoter regions (Figs 5A, B, D and S5A-B) and can activate transcription when artificially tethered to promoters (Fig. 5E-G). Third, DFs are required for transcriptional activation (as well as for the decay) of ncRNAs in a manner similar to that of mRNAs (Fig S2G-I). Fourth, transcription and/or decay of ncRNAs seems to relate mostly to environmentally induced genes and involves only Xrn1p and Dcp2p (Geisler et al., 2012), whereas we show that transcription of all genes is affected by DFs (Figs. 1D and S1C-D) and that all DFs examined are shuttling proteins (Fig. 4 and S4) and several of them bind chromatin and activate transcription. Last, in our strain background, there is a significant difference in the transcriptional capacity of cells expressing the enzyme dead Dcp2-4p or Xrn1^{D208A}p and those carrying a deletion of

DCP2 or *XRN1* (Figs. 2 and S2). This difference is inconsistent with a simple decapping and degradation of ncRNA as the main underlying mechanism. Indeed, inactivating the enzymatic activity of Dcp2p, using Dcp2-4p mutant form, does not affect the protein capacity to activate transcription in the tethering assay (Figs. 5E-F and S5E and Table S5), demonstrating that the decapping activity of Dcp2p is not necessary for its capacity to stimulate transcription in this assay.

Nevertheless, it is quite possible that the effect of the decaysome on mRNA synthesis involves more than one mechanism, a general and direct one described here, and one that acts indirectly through degradation of ncRNA, which may be restricted to subclasses of genes. Some of our unpublished observations suggest that the relative impact of the two mechanisms is strain dependent.

The involvement of the studied DFs in transcription, in a manner dependent on proper mRNA decay, reveals the circular nature of the gene expression process (Fig. 7C). Remarkably, the link between transcription and mRNA decay machineries is bilateral, as Pol II controls cytoplasmic mRNA decay (Goler-Baron et al., 2008; Harel-Sharvit et al., 2010; Shalem et al., 2011). Cyclic processes are inherently robust, because defects in one stage affect the overall pace of the entire process, thereby maintaining the essential balance between the stages. The maintenance of mRNA levels is one manifestation of this principle.

Experimental procedures

Yeast strains and plasmids.

Lists of yeast strains, plasmids, construction details and proliferation details can be found in the Supplementary Information.

Fluorescence microscopy.

Fluorescence microscopy was performed as previously described (Lotan et al., 2005).

Fluorescent *in situ* hybridization (FISH).

FISH probes were designed as described previously (Levsky et al., 2002). FISH was performed essentially as described (Zenklusen et al., 2008). Images were analyzed by a 2D Gaussian fit algorithm as previously described (Thompson et al., 2002; Zenklusen et al., 2008). A detailed protocol, including image acquisition, data analysis, three dimensional (3D) reconstructions and statistical analysis can be found in Supplementary Information.

Genomic run-on (GRO), 3'/5' ratio analysis and RNA pol II ChIP on chip (RPCC) experiments.

Genomic run-on (GRO) analysis (three independent experiments) was performed as previously described (Garcia-Martinez et al., 2004; Pelechano and Perez-Ortin, 2010), with modifications (García-Martínez et al., 2011) using an updated version of the nylon macroarrays (Alberola et al., 2004). 3'/5' ratio analyses and RPCC were performed

essentially as previously described (Pelechano et al., 2009; Rodriguez-Gil et al., 2010). Detailed protocols can be found in Supplementary information.

Run-on of *GAL1*

Slot-blotted membranes were performed as previously described (Rodriguez-Gil et al., 2010). 300 bp-long DNA probes were obtained by PCR. Midpoints of the probes for *GAL1* were: +109 (5'); +871 (middle); and +1582 (3'), relative to the transcription start site. Run-on assays, hybridizations and genomic DNA labeling were done as described (Rodriguez-Gil et al., 2010).

Chromatin Immuno-precipitation (ChIP) with TAP tagged proteins.

Recruitment of TAP-tagged proteins to chromatin was assayed by ChIP analysis as previously described (Buck and Lieb, 2006) with some modifications, as detailed in Supplementary Information.

Real-time PCR (qPCR).

The Absolute blue SYBR Green ROX mix (Thermo Scientific) was used for qPCR according to the manufacturer's instructions. qPCR was performed in Rotor-Gene 6000 (Corbett Life Science, Sydney, Australia). Details can be found in the Supplementary Information.

Tethering DFs to promoters.

To assess stimulation of transcription, strains expressing DFs fused to Gal4p-BD were subjected to two assays:a β-gal assay (Paz et al., 1999) and Northern analysis. As a negative control we used cells expressing Gal4p-BD alone ("vector"), or fused to the

non-DF proteins Hsp104p, Tor1p, Rad17p, Elg1p or Dot1p. As a positive control we used Gal4p-BD fused to Rpb3p, which was previously shown to strongly stimulate transcriptionin this assay (Titz et al., 2006).

Statistical analysis of nuclear localization and β-gal assays: χ^2 test and standard t-test were used, respectively, followed by p-value calculations using GraphPad Software (http://www.graphpad.com/quickcalcs/pvalue1.cfm).

Primary accessions

Gene Expression Omnibus (GEO) database reference for all genomic data is series GSE29519

References

Alberola, T.M., Garcia-Martinez, J., Antunez, O., Viladevall, L., Barcelo, A., Arino, J., and Perez-Ortin, J.E. (2004). A new set of DNA macrochips for the yeast Saccharomyces cerevisiae: features and uses. Int Microbiol *7*, 199-206.

Anderson, J.S., and Parker, R.P. (1998). The 3' to 5' degradation of yeast mRNAs is a general mechanism for mRNA turnover that requires the SKI2 DEVH box protein and 3' to 5' exonucleases of the exosome complex. Embo J *17*, 1497-1506.

Badis, G., Saveanu, C., Fromont-Racine, M., and Jacquier, A. (2004). Targeted mRNA degradation by deadenylation-independent decapping. Mol Cell *15*, 5-15.

Bataille, A.R., Jeronimo, C., Jacques, P.E., Laramee, L., Fortin, M.E., Forest, A., Bergeron, M., Hanes, S.D., and Robert, F. (2012). A Universal RNA Polymerase II CTD Cycle Is Orchestrated by Complex Interplays between Kinase, Phosphatase, and Isomerase Enzymes along Genes. Mol Cell *45*, 158-170.

Brune, C., Munchel, S.E., Fischer, N., Podtelejnikov, A.V., and Weis, K. (2005). Yeast poly(A)-binding protein Pab1 shuttles between the nucleus and the cytoplasm and functions in mRNA export. RNA *11*, 517-531.

Buck, M.J., and Lieb, J.D. (2006). A chromatin-mediated mechanism for specification of conditional transcription factor targets. Nat Genet *38*, 1446-1451.

Chang, J.H., Xiang, S., Xiang, K., Manley, J.L., and Tong, L. (2011). Structural and biochemical studies of the 5'-->3' exoribonuclease Xrn1. Nat Struct Mol Biol *18*, 270-276.

Cheung, A.C., and Cramer, P. (2011). Structural basis of RNA polymerase II backtracking, arrest and reactivation. Nature *471*, 249-253.

Churchman, L.S., and Weissman, J.S. (2011). Nascent transcript sequencing visualizes transcription at nucleotide resolution. Nature *469*, 368-373.

Coller, J., and Parker, R. (2004). Eukaryotic mRNA decapping. Annu Rev Biochem *73*, 861-890.

Dunckley, T., and Parker, R. (1999). The DCP2 protein is required for mRNA decapping in Saccharomyces cerevisiae and contains a functional MutT motif. EMBO J *18*, 5411-5422.

Femino, A.M., Fay, F.S., Fogarty, K., and Singer, R.H. (1998). Visualization of single RNA transcripts in situ. Science *280*, 585-590.

Fish, R.N., and Kane, C.M. (2002). Promoting elongation with transcript cleavage stimulatory factors. Biochim Biophys Acta *1577*, 287-307.

Garcia-Martinez, J., Aranda, A., and Perez-Ortin, J.E. (2004). Genomic run-on evaluates transcription rates for all yeast genes and identifies gene regulatory mechanisms. Mol Cell *15*, 303-313.

García Martínez, J., Pelechano, V. and Pérez-Ortín, J.E. (2011). Genomic methods for evaluating transcription rates in Yeast Genetic Networks, A. Becskei, ed. (Totowa, NJ, Humana Press), pp. 25-44.

Garneau, N.L., Wilusz, J., and Wilusz, C.J. (2007). The highways and byways of mRNA decay. Nat Rev Mol Cell Biol *8*, 113-126.

Geisler, S., Lojek, L., Khalil, A.M., Baker, K.E., and Coller, J. (2012). Decapping of Long Noncoding RNAs Regulates Inducible Genes. Mol Cell *45*, 279-291.

Goler-Baron, V., Selitrennik, M., Barkai, O., Haimovich, G., Lotan, R., and Choder, M. (2008). Transcription in the nucleus and mRNA decay in the cytoplasm are coupled processes. Genes Dev *22*, 2022-2027.

Grigull, J., Mnaimneh, S., Pootoolal, J., Robinson, M.D., and Hughes, T.R. (2004). Genome-wide analysis of mRNA stability using transcription inhibitors and microarrays reveals posttranscriptional control of ribosome biogenesis factors. Mol Cell Biol *24*, 5534-5547.

Harel-Sharvit, L., Eldad, N., Haimovich, G., Barkai, O., Duek, L., and Choder, M. (2010). RNA Polymerase II Subunits Link Transcription and mRNA Decay to Translation. Cell *143*, 552-563.

Hartzog, G.A., Wada, T., Handa, H., and Winston, F. (1998). Evidence that Spt4, Spt5, and Spt6 control transcription elongation by RNA polymerase II in Saccharomyces cerevisiae. Genes Dev *12*, 357-369.

He, F., Li, X., Spatrick, P., Casillo, R., Dong, S., and Jacobson, A. (2003). Genome-wide analysis of mRNAs regulated by the nonsense-mediated and 5' to 3' mRNA decay pathways in yeast. Mol Cell *12*, 1439-1452.

Jinek, M., Coyle, S.M., and Doudna, J.A. (2011). Coupled 5' nucleotide recognition and processivity in Xrn1-mediated mRNA decay. Mol Cell *41*, 600-608.

Kim, B., Nesvizhskii, A.I., Rani, P.G., Hahn, S., Aebersold, R., and Ranish, J.A. (2007). The transcription elongation factor TFIIS is a component of RNA polymerase II preinitiation complexes. Proc Natl Acad Sci U S A *104*, 16068-16073.

Komili, S., and Silver, P.A. (2008). Coupling and coordination in gene expression processes: a systems biology view. Nat Rev Genet *9*, 38-48.

Kruk, J.A., Dutta, A., Fu, J., Gilmour, D.S., and Reese, J.C. (2011). The multifunctional Ccr4-Not complex directly promotes transcription elongation. Genes Dev *25*, 581-593.

Levsky, J.M., Shenoy, S.M., Pezo, R.C., and Singer, R.H. (2002). Single-cell gene expression profiling. Science *297*, 836-840.

Lohr, D., Venkov, P., and Zlatanova, J. (1995). Transcriptional regulation in the yeast GAL gene family: a complex genetic network. FASEB J *9*, 777-787.

Lotan, R., Bar-On, V.G., Harel-Sharvit, L., Duek, L., Melamed, D., and Choder, M. (2005). The RNA polymerase II subunit Rpb4p mediates decay of a specific class of mRNAs. Genes Dev *19*, 3004-3016.

Lotan, R., Goler-Baron, V., Duek, L., Haimovich, G., and Choder, M. (2007). The Rpb7p subunit of yeast RNA polymerase II plays roles in the two major cytoplasmic mRNA decay mechanisms. J Cell Biol *178*, 1133-1143.

Malagon, F., Kireeva, M.L., Shafer, B.K., Lubkowska, L., Kashlev, M., and Strathern, J.N. (2006). Mutations in the Saccharomyces cerevisiae RPB1 gene conferring hypersensitivity to 6-azauracil. Genetics *172*, 2201-2209.

Mason, P.B., and Struhl, K. (2005). Distinction and relationship between elongation rate and processivity of RNA polymerase II in vivo. Mol Cell *17*, 831-840.

Meinhart, A., Kamenski, T., Hoeppner, S., Baumli, S., and Cramer, P. (2005). A structural perspective of CTD function. Genes Dev *19*, 1401-1415.

Morillo-Huesca, M., Vanti, M., and Chavez, S. (2006). A simple in vivo assay for measuring the efficiency of gene length-dependent processes in yeast mRNA biogenesis. Febs J *273*, 756-769.

Muhlrad, D., and Parker, R. (1999). Recognition of yeast mRNAs as "nonsense containing" leads to both inhibition of mRNA translation and mRNA degradation: implications for the control of mRNA decapping. Mol Biol Cell *10*, 3971-3978.

Muhlrad, D., and Parker, R. (2005). The yeast EDC1 mRNA undergoes deadenylation-independent decapping stimulated by Not2p, Not4p, and Not5p. EMBO J *24*, 1033-1045.

Munchel, S.E., Shultzaberger, R.K., Takizawa, N., and Weis, K. (2011). Dynamic profiling of mRNA turnover reveals gene-specific and system-wide regulation of mRNA decay. Mol Biol Cell *22*, 2787-2795.

Page, A.M., Davis, K., Molineux, C., Kolodner, R.D., and Johnson, A.W. (1998). Mutational analysis of exoribonuclease I from Saccharomyces cerevisiae. Nucleic Acids Res *26*, 3707-3716.

Paz, I., Meunier, J.R., and Choder, M. (1999). Monitoring dynamics of gene expression in yeast during stationary phase. Gene *236*, 33-42.

Pelechano V and Pérez-Ortín, J.E. (2008). The transcriptional inhibitor thiolutin blocks mRNA degradation. Yeast 25, 85-92.

Pelechano, V., Jimeno-Gonzalez, S., Rodriguez-Gil, A., Garcia-Martinez, J., Perez-Ortin, J.E., and Chavez, S. (2009). Regulon-specific control of transcription elongation across the yeast genome. PLoS Genet *5*, e1000614.

Pelechano, V., and Perez-Ortin, J.E. (2010). There is a steady-state transcriptome in exponentially growing yeast cells. Yeast *27*, 413-422.

Perez-Ortin, J.E., de Miguel-Jimenez, L., and Chavez, S. (2011). Genome-wide studies of mRNA synthesis and degradation in eukaryotes. Biochim Biophys Acta. In press (PMID:22182827)

Rodriguez-Gil, A., Garcia-Martinez, J., Pelechano, V., Munoz-Centeno Mde, L., Geli, V., Perez-Ortin, J.E., and Chavez, S. (2010). The distribution of active RNA polymerase II along the transcribed region is gene-specific and controlled by elongation factors. Nucleic Acids Res *38*, 4651-4664.

Shalem, O., Dahan, O., Levo, M., Rodriguez Martinez, M., Furman, I., Segal, E., and Yitzhak Pilpel, Y. (2008). Transient transcriptional responses to stress are generated by opposing effects of mRNA production and degradation. Mol Syst Biol. *4*, 223.

Shalem, O., Groisman, B., Choder, M., Dahan, O., and Pilpel, Y. (2011). Transcriptome kinetics is governed by a genome-wide coupling of mRNA production and degradation: a role for RNA Pol II. PLoS Genet *7*, e1002273.

Solinger, J.A., Pascolini, D., and Heyer, W.D. (1999). Active-site mutations in the Xrn1p exoribonuclease of Saccharomyces cerevisiae reveal a specific role in meiosis. Mol Cell Biol *19*, 5930-5942.

Teixeira, D., and Parker, R. (2007). Analysis of P-body assembly in Saccharomyces cerevisiae. Mol Biol Cell *18*, 2274-2287.

Thompson, N.L., Lieto, A.M., and Allen, N.W. (2002). Recent advances in fluorescence correlation spectroscopy. Curr Opin Struct Biol *12*, 634-641.

Titz, B., Thomas, S., Rajagopala, S.V., Chiba, T., Ito, T., and Uetz, P. (2006). Transcriptional activators in yeast. Nucleic Acids Res *34*, 955-967.

van Dijk, E.L., Chen, C.L., d'Aubenton-Carafa, Y., Gourvennec, S., Kwapisz, M., Roche, V., Bertrand, C., Silvain, M., Legoix-Ne, P., Loeillet, S.*, et al.* (2011). XUTs are a class of Xrn1-sensitive antisense regulatory non-coding RNA in yeast. Nature *475*, 114-117.

Velculescu, V.E., Zhang, L., Zhou, W., Vogelstein, J., Basrai, M.A., Bassett, D.E., Jr., Hieter, P., Vogelstein, B., and Kinzler, K.W. (1997). Characterization of the yeast transcriptome. Cell *88*, 243-251.

Villa, T., Ceradini, F., and Bozzoni, I. (2000). Identification of a novel element required for processing of intron-encoded box C/D small nucleolar RNAs in Saccharomyces cerevisiae. Mol Cell Biol *20*, 1311-1320.

Zenklusen, D., Larson, D.R., and Singer, R.H. (2008). Single-RNA counting reveals alternative modes of gene expression in yeast. Nat Struct Mol Biol *15*, 1263-1271.

Figure legends

Fig. 1. Transcription of most genes is down regulated in strains defective in 5'-3' mRNA decay. (**A**) Deletions of various mRNA decay factors do not lead to mRNA accumulation. Northern blot hybridization images of mRNAs from the indicated deletion strains (Genetic backgrounds: Strain 1: yMC229; strain 2: yMC370; strain 3: yMC375). The same membrane was probed with the indicated probes. Quantification of the signals in A is presented in Fig. S1A. (**B**) Decay of the indicated mRNAs at 30ºC was determined after blocking transcription by 1-10 phenanthroline (100µg/ml) (Grigull et al., 2004). Half-life (HL) was calculated as described in (Lotan et al., 2007). Additional decay experiments are shown in Figs. 2 and S2. **(C)** Scatter plot data from thiolutin shut-off assay (Pelechano et al., 2008) showing Log_2 ratios (Δ*xrn1*/WT) of HL vs. mRNA steady state level before drug addition (RA). Spots bellow the yellow line and on the right side of the red line represent mRNAs whose RA decreased and stability increased. The percentage of genes in each quadrant is indicated. (**D**) Changes in transcription rates in Δ*xrn1* cells. Scatter plot of the GRO signals in the mutants relative to WT, plotted as a function of the signal in the WT. A value below zero (red horizontal line) indicates defective transcription in the mutant. The black line represents the fitted linear with the equations shown in top right corner of each panel. Yellow line represents the median values. See also Fig. S1 and Tables S1-S2 and S4.

Fig. 2. Transcriptional induction by various inducers is dependent on enzymatically active Xrn1p and Dcp2p. Transcriptional induction of *GAL* genes (**A**) and decay of *GAL* mRNAs (**B**) was performed on the indicated strains as described in Experimental procedures. Shown are Northern blot images (left panel) and

quantification (right panels), performed as in Fig. S1 except that results are shown as percentage relative to time point 20 min of WT (in A) or 0 min of each strain (in B). (**C**) Northern analysis showing induction of the indicated HS genes by temperature shift up. Quantification was performed as in Fig 2A. (**D**) To examine mRNA decay, transcription of the indicated HS genes was inhibited by shifting the temperature down, and the levels of the indicated mRNAs were monitored by Northern analysis and quantified as in Fig 2B. *SCR1* RNA is shown for loading control, and was used for normalization. Error bars represent SD of three assays. See also Fig. S2.

Fig. 3. Xrn1p affects Pol II occupancy on *TEF4* gene. (**A**) Schematic representation of the FISH approach and the position of the six probes. Following splicing of *TEF4* transcript, the intron is processed into the nucleolar associated-*snR38* (Villa et al., 2000), whose detection is used as an internal control for the hybridization efficiency. This was especially helpful in cases where no TS signal was detected. (**B**) Merged FISH images of several representative cells with or without TSs. Images of *TEF4* Cy5 labelled probes, *snR38* Cy3 labelled probe, DAPI (pseudocolored green, red and blue, respectively) and spot centroids (white dots; see Fig. S4A) were merged into single images. Arrows indicate TSs. The large red area is the nucleolus. Note that the probe that detects the intron is only seen in the contexts of the TS or the nucleolus. It was never seen in the cytoplasm. (**C**) A single three dimensional (3D) image of *TEF4* mRNA (green spots) and the cell nucleus stained by DAPI (blue area) showing only a single FISH spot in the nucleus (indicated by red arrow). See also Movies S1 to S3. (**D**) Interpretation of transcription site intensities. Upper panel: example of distribution of the transcription site intensity (x axis) in WT cells. Results are represented by the histogram, in percentages of WT cells (y axis). For comparison, the superimposed blue

curve corresponds to the distribution of the intensities of all the FISH spots in WT, as shown in Fig. S4B. The first column corresponds to cells without any FISH spot in the nucleus, to which the algorithm attributed a TS intensity of 0. The areas designated I, II and III, depicted above the histogram, refer to the interpretations and cell images in the panels below. (I) Cells without any FISH spots in the nucleus were interpreted as cells without any active transcription of the *TEF4* gene at the time of the fixation. Two examples of such cells are shown in panels a and b. Optical sectioning technology indicated that all the spots are above or below the nucleus. (II) Cells with a low intensity FISH spot in the nucleus, which corresponds to the value of a single mRNA in the cytoplasm (as determined in Fig. S4B). This cell population is interpreted as occupying a single elongating Pol II at the *TEF4* gene. Two examples of such cells are shown in panels c and d. Arrows indicate the TSs. In panel d, the other spots that appear inside the nucleus are either above or under it (as indicated by the optical sectioning technology). (III) Cells with high intensity FISH spots in the nucleus. This cell population has multiple nascent *TEF4* mRNAs in the TS; hence their *TEF4* gene occupiesmore than one elongating Pol II simultaneously. Two examples of such cells are shown (panels e and f). Arrows indicate TSs; Scale bar, 1 μm. (**E-G**) Frequency of cells (y axis) as a function of *TEF4* TSs intensities. See section D above for interpretation. *p=2.6x10^{-8} between WT and *xrn1*^{D208A}; **p<10^{-4} between WT and both *xrn1* mutants. See also Fig. S3.

Fig. 4. **Factors of the major mRNA decay pathway are nucleocytoplasmic shuttling proteins, whose import is compromised by mutating the Xrn1p active site.** (**A**) WT cells or *xpo1-1, mex67-5* mutant cells co-expressing Pab1p-GFP and the indicated RFP fusion proteins were proliferated at 24°C and then shifted to 37°C for 1 h (II, IV-V) or 2

h (VII, IX-X). Cycloheximide (CHX; 100µg/ml) was included, as indicated, immediately before the temperature shift-up. Pab1p-GFP was used to determine the efficiency of the assay and to serve as a nuclear marker (Brune et al., 2005). In all cases, Pab1p-GFP was present in the nuclei of at least 40% of the heat inactivated mutant cells. Arrows indicate nuclear co-localization of Pab1p-GFP and RFP fusion proteins. The images in (IX) are a composition of two different fields. (**B-D**) Import of Xrn1p is dependent on Xrn1p exonuclease activity and on its 5'-phosphate binding. Δ*xrn1, xpo1-1, mex67-5*, cells co-expressing *XRN1*-GFP or the indicated mutant derivative thereof and *PAB1*-RFP (B), or *DCP2*-RFP (C), were subjected to the same assay as in panel A, IX (for B) or IV (for C and D). Results of Pab1p-RFP, which was co-expressed with Xrn1p-GFP, and Pab1p-GFP that was co-expressed with Dcp2p-RFP in the Δ*xrn1* mutant, are shown in D. Percentage of cells with nuclear localization was determined. Mean values ±SD are shown (N >100). P-values of any pairwise difference that was <0.05 is indicated. All other differences were statistically insignificant. See also Fig. S4.

Fig. 5. Factors of the major mRNA decay pathway associate with chromatin of transcriptionally active genes and can stimulate transcription upon recruitment to reporter promoters. (**A**) Association of Xrn1p across the *PMA1* gene. ChIP-TAP analysis of WT cells expressing Rpb3p-TAP (a Pol II subunit), Xrn1p-TAP or control cells without TAP (No-TAP) was performed and analyzed by qPCR with amplicons shown in the map (numbers represent the amplicon's middle nucleotide relative to the translation start site). Bottom panels show chromatin association relative to amplicon 115 (7.1±2.6 fold of No-TAP; taken as 100%). Mean values, normalized to the input signal, No-TAP signal and an internal *lacZ* spike ±SD are shown. The experiment with Xrn1p-TAP was performed in four biological repeats. (**B**) Xrn1p-TAP and Rpb3p-TAP

associate with the *TEF4* promoter, but not with rDNA. (**C**) Association of Xrn1p-TAP with *GAL1* chromatin is increased upon induction by galactose. Shown are the Log_2 ratios of Xrn1p-TAP ChIP signal in galactose vs. glucose for each amplicon indicated in the map. (**D**) The indicated DFs associate with *PMA1* promoter. B and C show qPCR results of the indicated amplicons, expressed as fold enrichment relative to the No-TAP control signal. Shown are mean values of three or more assays, normalized to the input signal and to an internal *lacZ* spike, ±SD. (**E**) Northern blot analysis using probes for the indicated mRNAs of WT cells expressing different Gal4p-BD fusion genes. The same membrane was probed with *GAL10* (shown in panel F), *HIS3*, *ACT1* and *SCR1*. Cells expressing Gal4p-BD-Rpb3p served as a positive control, and cells expressing Gal4p-BD-Hsp104p or vector alone served as negative controls. Additional negative controls are shown in Table S5. (**F**) Quantification of (A) by PhosphorImager. Results (average ± SD of three assays) were normalized to *SCR1* RNA level and are shown as fold induction (in log_{10} scale) relative to the mRNA level in cells carrying the vector only. (**G**) Northern blot images of the indicated mutant cells expressing the indicated Gal4p-BD fusions. The same membrane was probed with *HIS3* and *SCR1*. Compare to the expression in WT cells in panel E (All membranes were exposed to X-ray film in parallel). * Exposure time as in panel E. ** 1/3 exposure time. See also Fig. S5 and Table S5

Fig 6. Factors of the major mRNA decay pathway affect transcription elongation. (**A**) The impact of Xrn1 disruption on transcription is proportional to the ORF length. Sliding window analysis of the dependence of the change in TR ratio (mutant/WT) on ORF length. Genes were ordered according the ORF length (that coincides with the length of the probe in the macroarray). TR ratios in log_2 scale were averaged using a

200-gene sliding window. The red line shows the fitted linear negative tendency. The p-values shown at the top were obtained by t-test determining the differences in average TR ratio between the genes of < 1000 pb and those > 1750 bp. (**B**) Left columns (blue): Pol II ChIP was performed, the DNA was labeled and hybridized to probes representing 5' portions and 3' portions of 384 genes, as described in supplemental experimental procedures. The histogram depicts the average ratio of 3'/5' signals obtained for any of the indicated strain. Right columns (red): Distribution of Pol II capable of elongating transcription *in vitro*, determined by run-on followed by hybridization to the same membrane (after stripping off the probes) described earlier. The average ratio of 3'/5' signals is shown. A Wilcoxon test shows that the medians of the distributions are different for total Pol II molecules but not for elongating ones. (**C**) Log_2 representation of Rpb3p-TAP and Ser-2-phosphorylated CTD (Ser2P-CTD) ChIP signal at the indicated positions along *GAL1* in cells grown in galactose medium. Data are expressed relative to amplicon "28", followed by normalization of each value to the corresponding position in the WT strain, which was defined as "1". Mean values and SD of three independent experiments are shown. See also Fig. S6.

Fig. 7. Coordination between transcription and decay. (**A**) A correlation between mRNA stability and synthesis is observed by disrupting *XRN1*. Box plot representation of the median and 2nd and 3rd quartiles of the changes in transcription rate (TR) of two gene categories: moderate decrease in degradation rate (DR) and strong decrease in DR (see Table S4). DR was calculated as described in experimental procedures section. The whiskers show the maximum and minimum of the data set, excluding the outliers which

lie beyond the 1.5 times the interquartile range. Distributions were found to be different using Wilcoxon statistical test as shown in the upper part at the indicated p-value. (**B-C**) Transcriptional induction of *GAL* genes (B) and decay of *GAL* mRNAs (C) was performed on the indicated strains as described in Fig 2A-B. Shown are Northern blot images (left panel) and quantification (right panels). The Xrn1p proteins in the different strains were expressed as GFP fusion proteins, encoded on the centromeric plasmids pMC491, pMC492, pMC579 and pMC582, in an otherwise genomic Δ*xrn1* (yMC511). (**D**) **A conceptual model:** Gene expression is a circular process (see Discussion).

Figure 1

Click here to download Figure: Haimovich fig 1 revised 23.2.12 (Motti).pdf

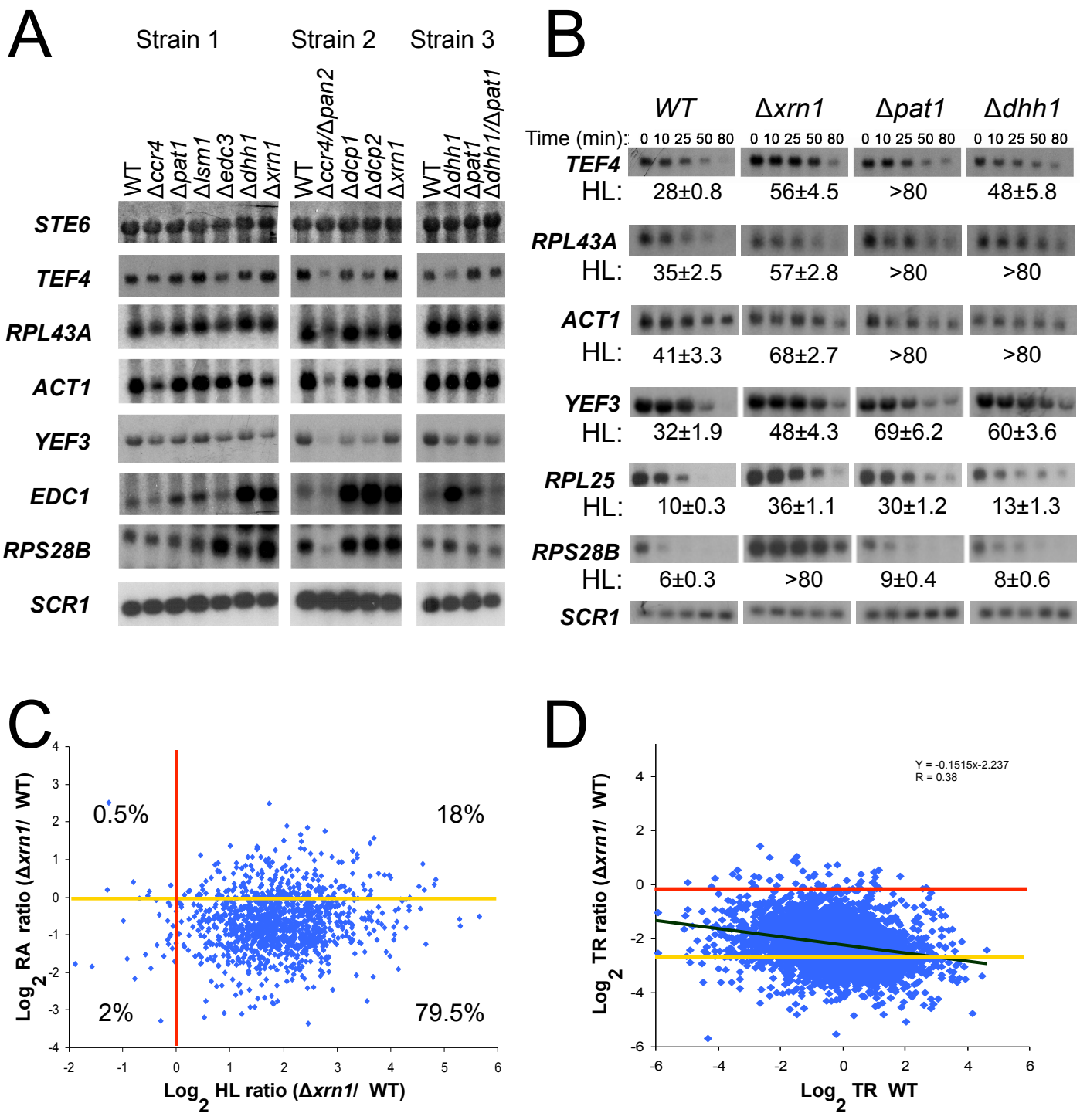

Figure 2

Click here to download Figure: Haimovich fig 2 reduced size.pdf

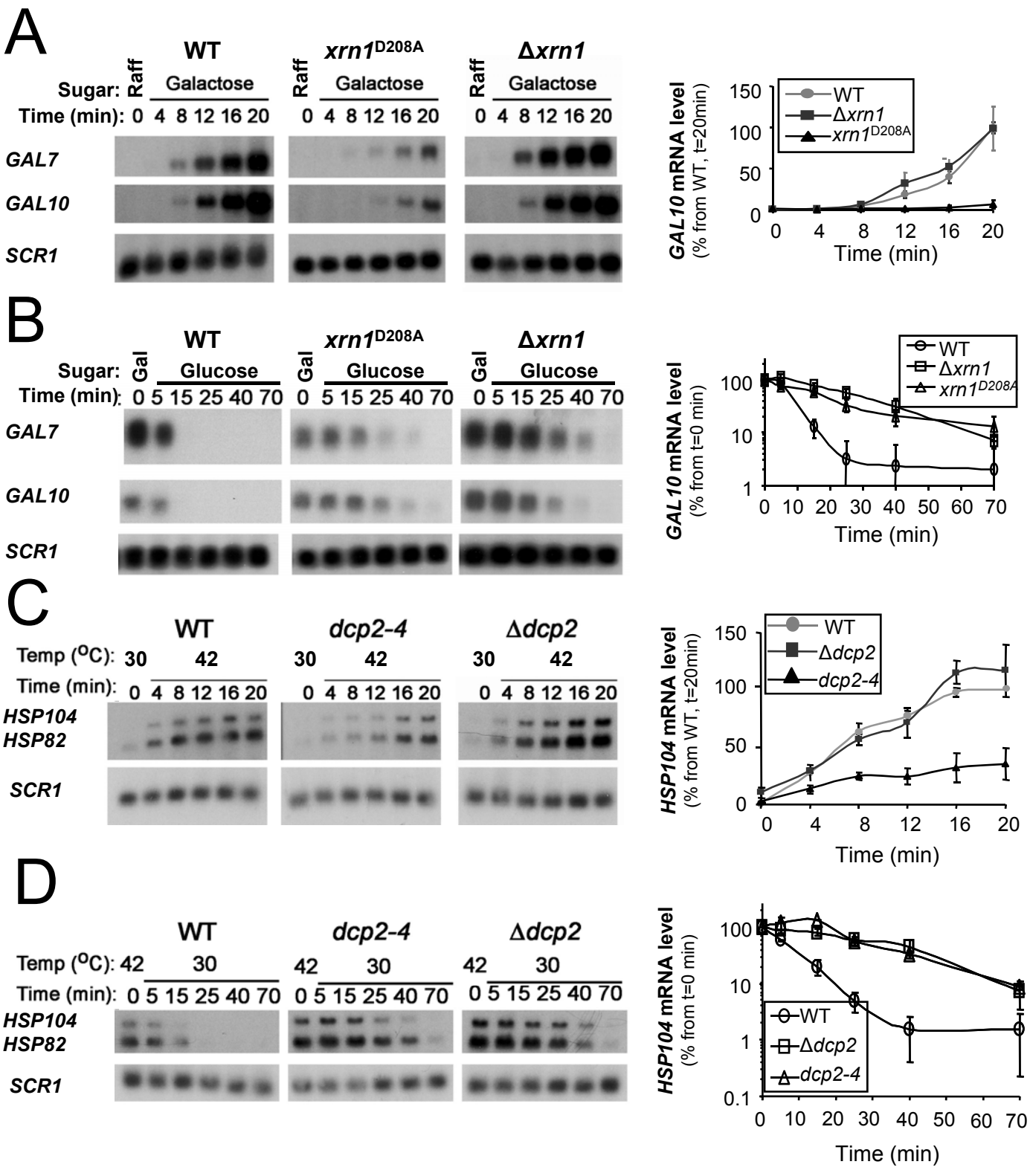

Figure 3

Click here to download Figure: Haimovich fig 3.pdf

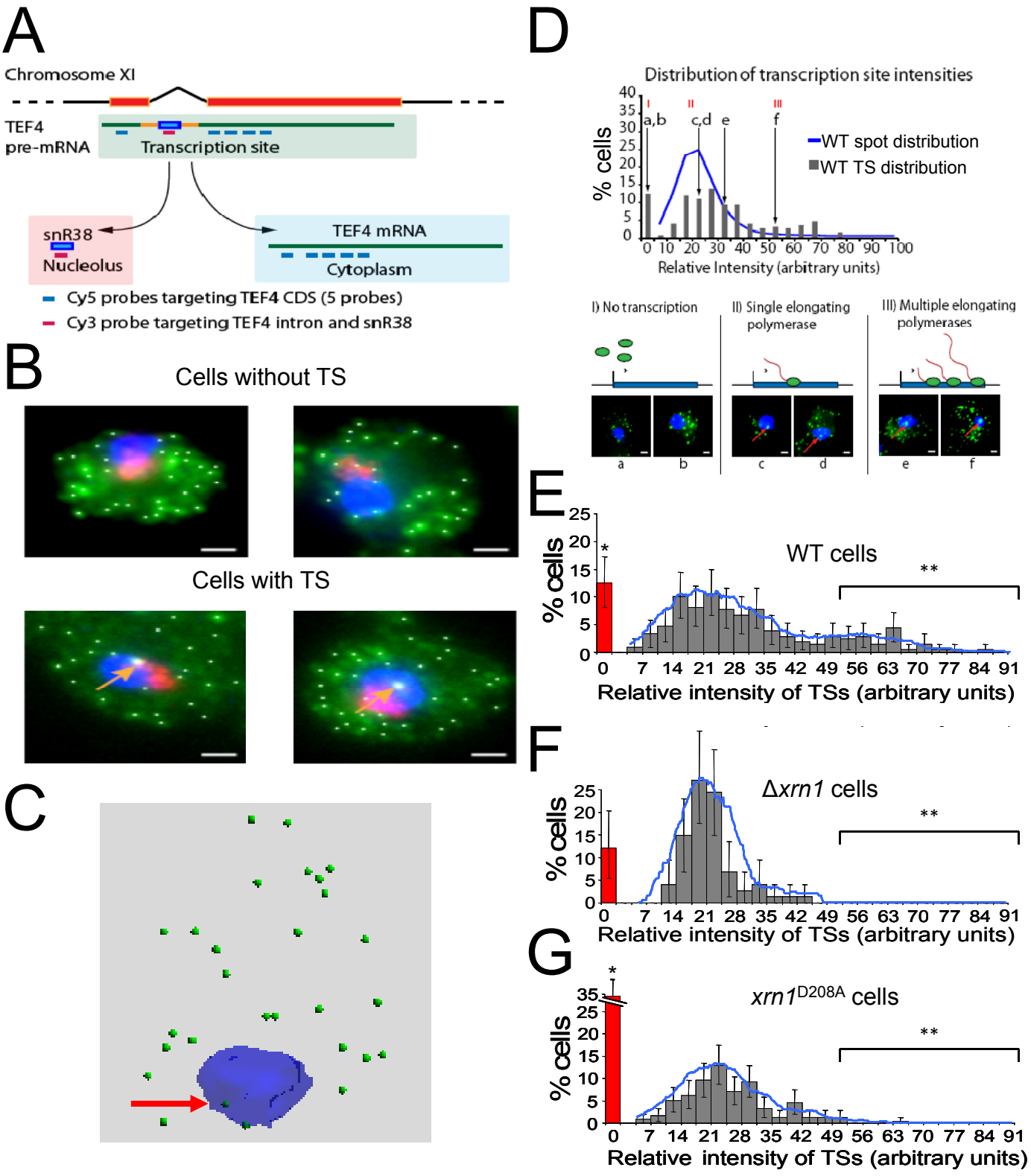

Figure 4

Click here to download Figure: Haimovich fig 4 29-2-12.pdf

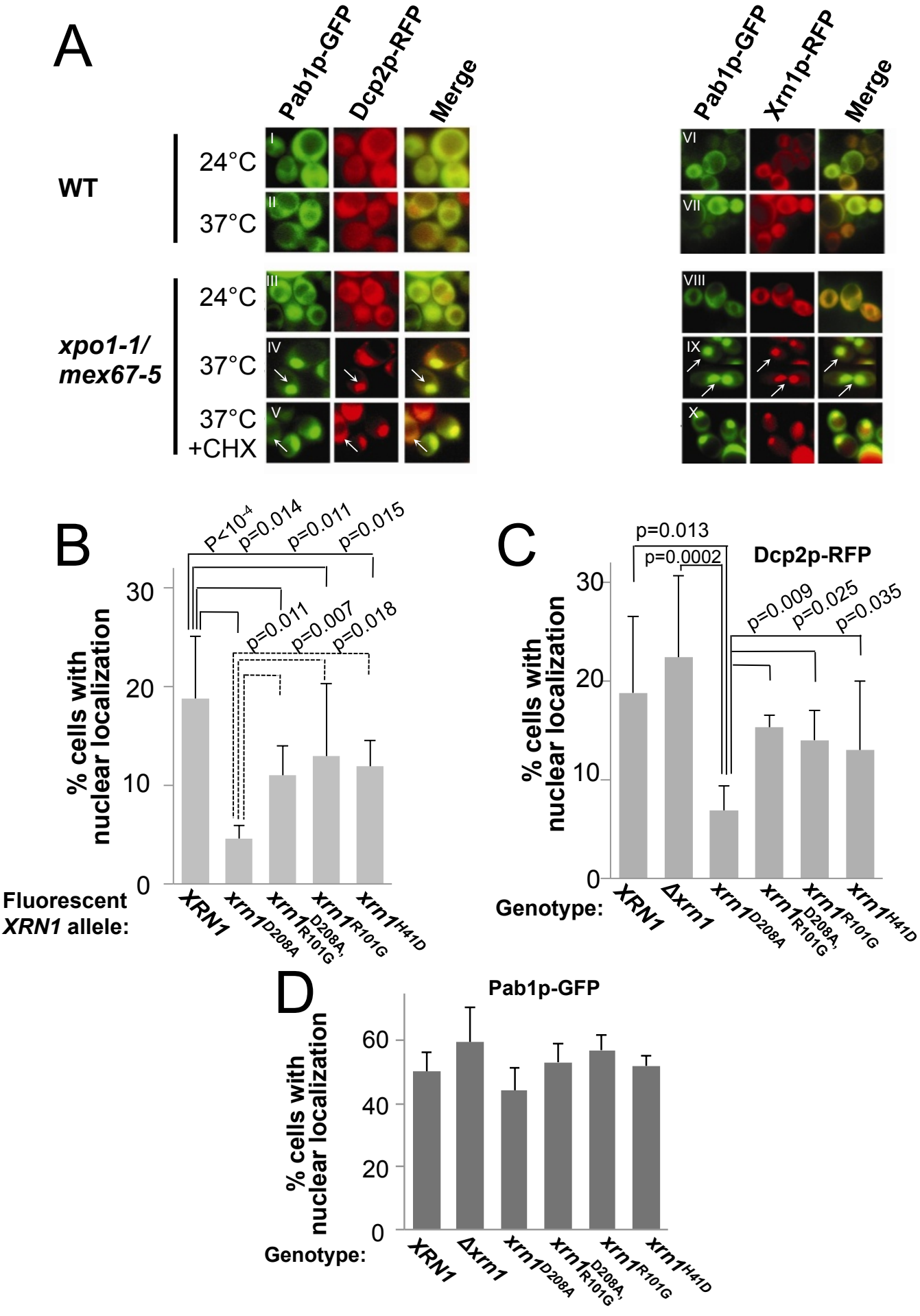

Figure 5

Click here to download Figure: Haimovich fig 5 revised 26.2.12.pdf

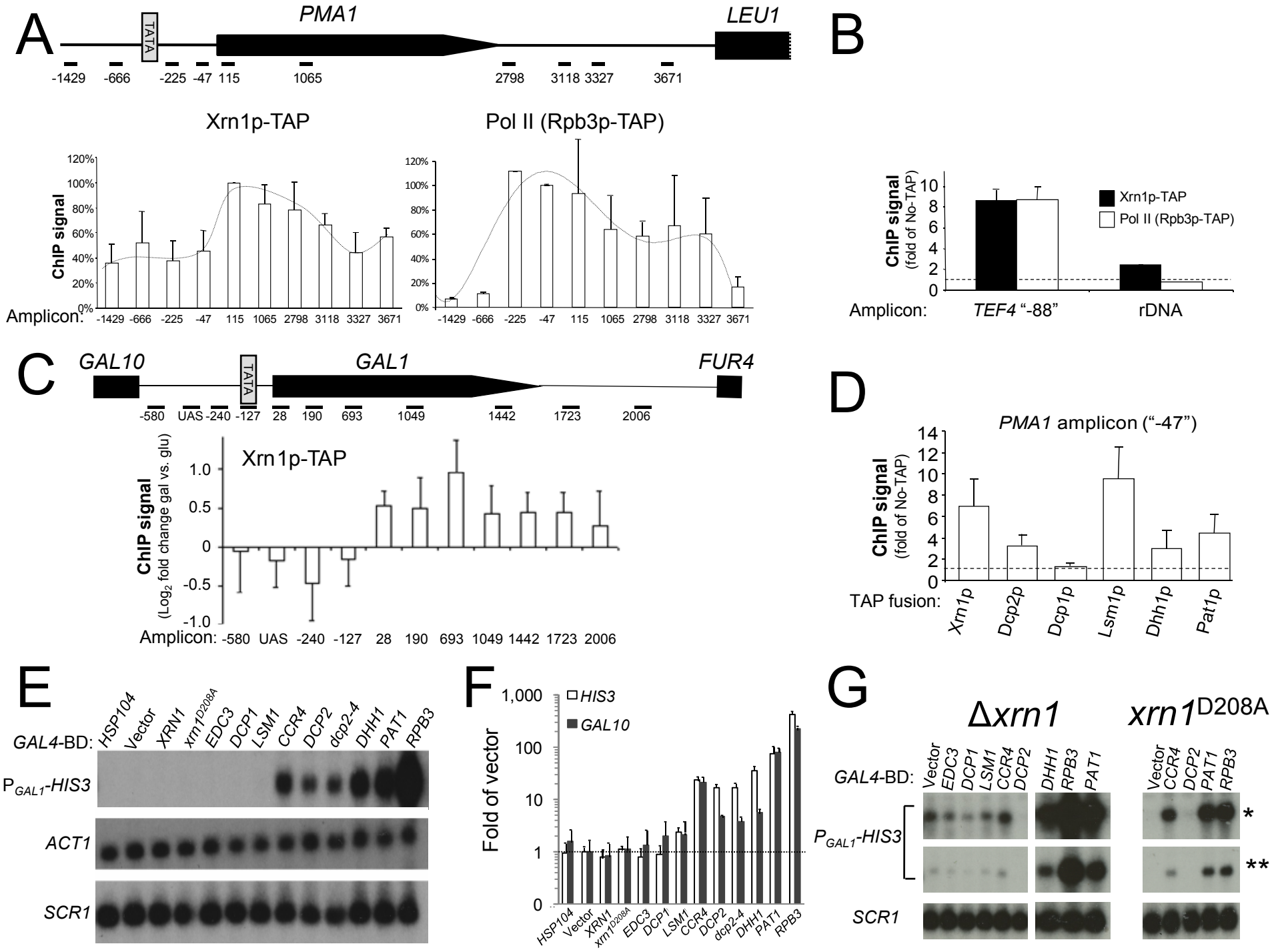

Figure 6

Click here to download Figure: haimovich fig 6 elongation figure 23.2.12 (Motti).pdf

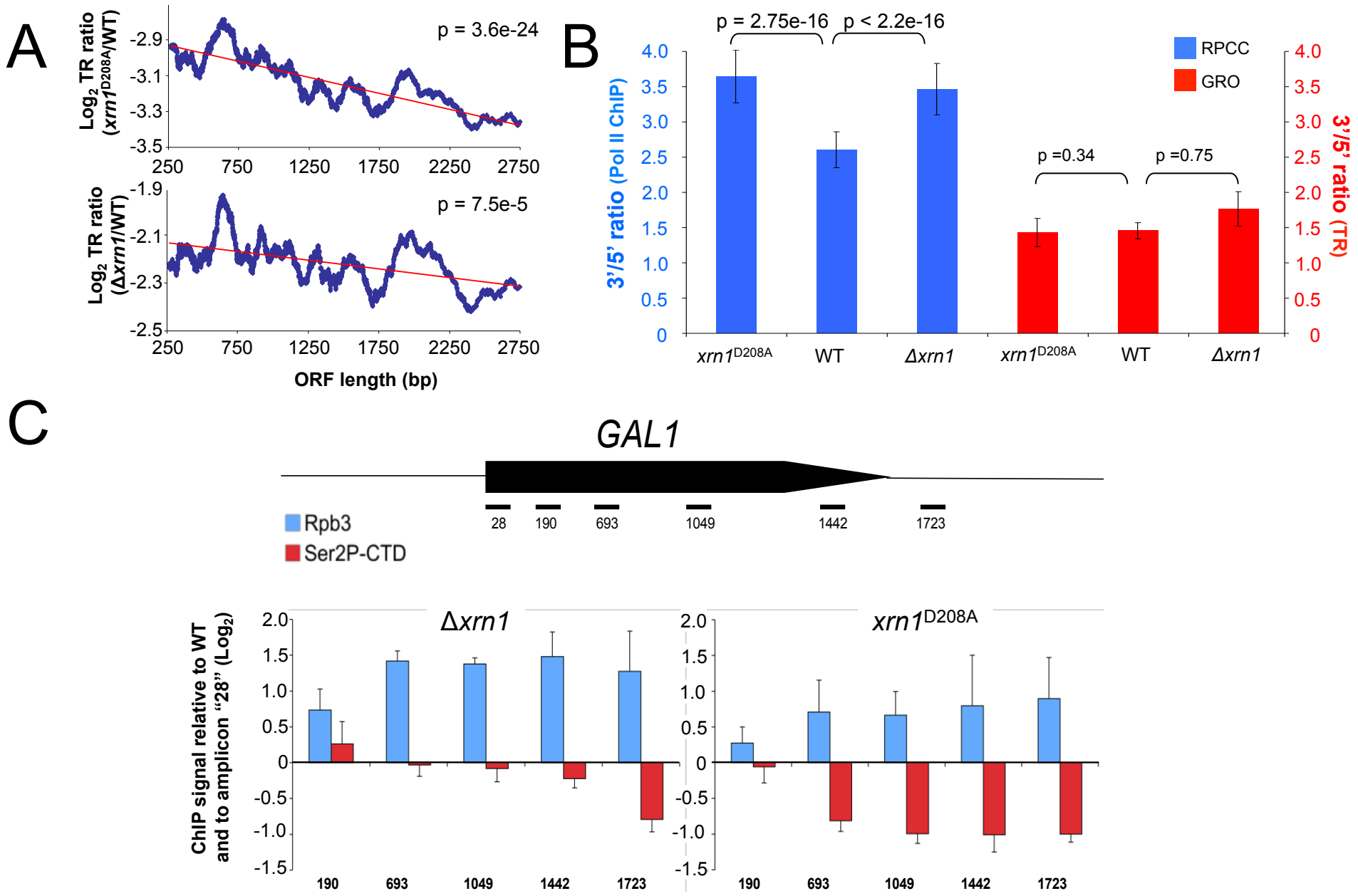

Figure 7

Click here to download Figure: Haimovich fig 7 revised 19.2.12.pdf

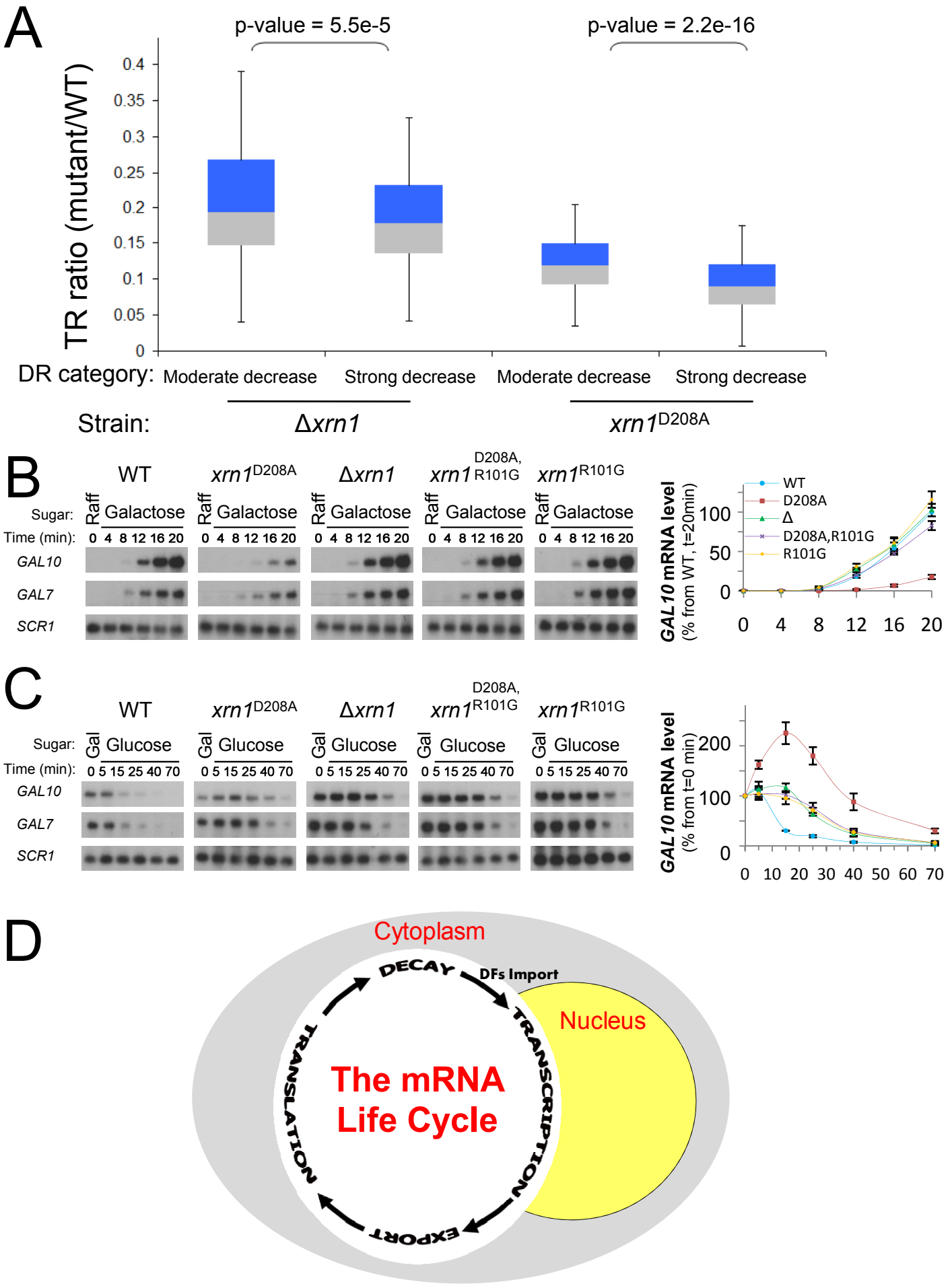

Supplementary Information

Supplementary Figure legends

Fig. S1, related to Fig. 1 and tables S1 to S5: mRNA decay mutants exhibit reduced transcription, which may be related to interactions with nuclear factors, but not to proliferation or PBs formation. (**A**) Deletion mutants from four different genetic backgrounds (the WT of strains 1, 2, 3 and 4 are yMC229, yMC370, yMC375 and yMC458, respectively) were allowed to proliferate in a synthetic complete (SC) medium till $1x10^7$ cells/ml. Cells were harvested and mRNA levels were assessed by Northern blot analysis with various probes, as indicated in the inset, followed by quantification with PhosphorImager. Results were normalized to those of *SCR1* and shown as percentages of WT levels (defined arbitrarily as 100%). Error bars represent SD of at least three assays. See also Fig. 1 for Northern blot images of some of the probes. **(B)** Map of the Physical and Genetic interactions between factors of the major cytoplasmic mRNA decay pathway and factors involved in the nuclear stages of gene expression. Data from Table S3 is represented as a map created by Cytoscape software (Shannon et al., 2003). Decay factors are represented by white diamonds. Red lines represent physical interactions, blue lines represent genetic interactions. (**C**) Changes in transcription rates in *xrn1*^{D208A} cells. Scatter plot of the GRO signals in the mutant relative to WT, plotted as a function of the signal in the WT. A value below zero indicates defective transcription in the mutant. Green line represents the fitted linear with the equation shown in top right corner of the panel. Yellow line represents the median values. (**D**) Changes in transcription rates in *xrn1* mutant cells. Bar graph of the Log_2 GRO signals in the mutants

relative to WT, plotted as a function of the number of genes. A value below zero (red line) indicates defective transcription. Note the shift to the left of the *xrn1*^{D208A} strain, indicating a more severe defect. (**E**) Proliferation rates of *xrn1* mutant strains. Upper image: strains yMC458 (WT), yMC459 (Δ*xrn1*) and yMC461 (*xrn1*^{D208A}) were spotted on YPD plates in a five-fold serial dilution (the first spot is 1x10^5 cells). Four biological repeats were made, which yielded similar results; only one is shown. The photo was taken after two days of proliferation at 28°C. Lower image: yMC511 (Δ*xrn1*) transformed with plasmids pMC491 (*XRN1*-GFP), pMC492 (*xrn1*^{D208A}-GFP), pMC582 (*xrn1*^{R101G}-GFP) or pMC579 (*xrn*^{D208A,R101G}-GFP) and yMC459 (Δ*xrn1*) were spotted on SC-ura as described for the upper image. Two biological repeats were made, which yielded similar results; only one is shown. (**F**) Accumulation of P-bodies (PBs) in *xrn1* mutant strains. The indicated strains, expressing Dhh1p-GFP, were grown under optimal conditions. Photos of cell samples without any treatment were taken, and the average number of Dhh1p-GFP containing PBs per cell ±SD was calculated (N>100).

Fig. S2, related to Fig. 2: Enzymatically active Xrn1p or Dcp2p are required for transcription and mRNA decay of HS, non-HS and non-coding genes. (**A**) Northern blot showing induction of *HSP26* by temperature shift up as described in Experimental procedures. Quantification was performed as in Fig 2A. (**B**) To examine mRNA decay, transcription of *HSP26* was inhibited by shifting the temperature down, and the levels of the indicated mRNAs were monitored by Northern analysis and quantified as in Fig 2B. *SCR1* RNA is shown for loading control, and was used for normalization. Error bars represent SD of three assays. (**C-F**) Transcriptional induction of *RPL43A* and *TEF4*

during recovery from 30 min HS at 42ºC was performed as described in Experimental procedures. **(C**) Northern blot showing *RPL43A* induction. Quantification of the results was done as in Fig. 2A, except that time 70 min of WT was set as 100%. Note that not only the induction in the *dcp2-4* strain is low (given the high level of their *RPL43A* mRNA at time 0 min), but it is also delayed by ~10 min. Note also that by 70 min following transcription induction, the *RPL43A* mRNA in WT and the *dcp2* mutants reached similar levels, reflecting the balance that starts to emerge between synthesis and decay, as the mRNA approaches its steady state level. This is in accordance with the results shown in Figs.1 and S1. **(D)** Cells were allowed to proliferate under optimal conditions (30ºC). To block transcription, cells were shifted to 42ºC (Lotan et al., 2005; Lotan et al., 2007) and mRNA degradation was monitored thereafter. Shown are Northern images and quantification as in Fig. 2B. **(E**) Northern blot images showing *TEF4* induction during recovery from 30 min HS at 42ºC . Quantification of the results was done as in C. (**F**) Decay of the *TEF4* mRNA at 30ºC was done as in Fig. 1B. Shown are Northern blot images and quantification as in Fig 2B. (**G**) Decay and (**H**) induction of the ncRNA *SUT508*/*TIR1axut* following HS and recovery from HS, respectively, was determined as for *RPL43A*. Panels A-B and E-F and panels C-D and G-H show experiments using the same set of yeast strains: (yMC458, yMC461 and yMC459 and yMC370, yMC374 and yGH177, respectively). (**I**) Decay of *SUT508* depends on *PAT1* and *DHH1*. Northern analysis of *SUT508* decay in the indicated strains was performed as in Fig 1B. *, ** - additional, unknown, RNAs detected by the probe. Note that the same RNAs, and an additional one, were also detected in the assay depicted in panels G-H (not shown). For all panels, *SCR1* RNA is shown for loading control, and was used for

normalization. Error bars represent SD of three assays.

Fig. S3, related to Fig. 3: The use of FISH to detect transcription sites (TSs) and to measure the number and distribution of *TEF4* mRNA molecules in single cells. (**A**) Quantitative single molecule analysis. **a**) FISH image showing single mRNAs detected as spots by *TEF4* specific Cy3 probes. Scale bar, 1 μm. **b**) Spot centroids. The raw image from panel a was analyzed using a 2D Gaussian fitting program (Zenklusen et al., 2008). See Experimental procedures for more details. **c**) Thresholded DAPI images, detecting nuclei of the cells in panel a. **d**) Images a, b and c (pseudocolored green, red and blue, respectively) were merged into a single image. (**B**) Distribution of FISH spots (most are cytoplasmic) according to their intensity. The intensity of the spots from various FISH experiments were normalized according to their median value and their distributions were plotted in percentages of total FISH spots, strain by strain. (**C**) Average number of *TEF4* mRNAs per cell (± SEM) as determined by FISH analysis. (**D**) Steady state level of *TEF4* mRNA as determined by Northern analysis. Quantification was done as in Fig. 1. Inset shows the Northern blot image of *TEF4,* and *SCR1* RNA as the loading control; Lane 1 - WT, lane 2 – Δ*xrn1*, lane 3 – $xrn1^{D208A}$. **(E to G)** Distribution of TS intensity (see also Fig. 3): comparison between WT and Δ*xrn1* cells (E), WT and $xrn1^{D208A}$ cells (F) and Δ*xrn1* and $xrn1^{D208A}$ cells (G). Error bars represent 95% confidence intervals. Numbers above bars represent p-values of the difference between the bins of the two strains calculated by resampling. An asterisk was added when the difference is significant ($P < 0.05$). The p value was calculated for the bin 38.5-91 as well, and is shown above each histogram**.** N > 200 cells, except for Δ*xrn1* cells (N=76). For more detailed description of

the statistical analysis see Experimental procedures.

Fig. S4, related to Fig. 4: Factors of the major mRNA decay pathway are nucleocytoplasmic shuttling proteins, **whose cellular localization can be affected by environmental conditions and genetic background**. (**A**) WT or *xpo1-1, mex67-5* strain expressing Pab1p-GFP and the indicated RFP fusion protein were treated as in Fig 3A. White arrows indicate example cases of nuclear co-localization of Pab1p-GFP (serving as a positive control (Brune et al., 2005) and RFP fusion proteins. Yellow arrows in VIII indicate a case of a cell whose nuclear localization of Edc3p-RFP, but not Pab1p-GFP, is observed already at the permissive temperature (24ºC) (observed in ~30% of the cells). (**B)** Δ*rpb4* strain expressing GFP-Rpb4p (a Pol II subunit) and Lsm1p-RFP were grown exponentially at 30°C. When the culture reached $1x10^7$ cells/ml (mid- exponential proliferation phase), the culture was starved for 1 h as described in Experimental procedures. Samples before ("Optimal") or after shifting to starvation conditions ("Starvation") were analyzed by fluorescence microscopy. Arrows indicate example cases of co-localization of GFP-Rpb4p and Lsm1p-RFP. At 1 h after shifting to starvation, GFP-Rpb4p can serve as a reliable nuclear marker (Selitrennik et al., 2006). Note that Lsm1p-RFP can be found in the nucleus also under optimal conditions (in ~40% of the cells). (**C**) Dcp2p-RFP is found in the nuclei of WT non-stressed cells in certain genetic backgrounds. WT strain expressing chromosomal *RPB6*-GFP (a Pol II subunit) and harboring *DCP2-RFP* was proliferated at 30°C. Exponentially proliferating cells ($1x10^7$ cells/ml) were inspected without further treatment. Rpb6p-GFP serves as a nuclear marker. Arrows indicate nuclear co-localization of Rpb6p-GFP and Dcp2p-RFP.

(**D, E**) Dcp2p-RFP and Ccr4p-RFP accumulate in the nuclei of starved WT cells. WT strain (yMC458) harboring GFP-*RPB4* and *DCP2*-RFP or *CCR4*-RFP were treated as in (B). Note that unlike the results shown in C, in this genetic background Dcp2p-RFP could not be detected in the nucleus unless the cells are starved. Arrows indicate example cases of nuclear co-localization of GFP-Rpb4p and the RFP fusion protein. (**F**) Lsm1p-RFP is found in the nuclei of heat-shocked WT cells. WT strain expressing chromosomal *RPB6*-GFP and harboring *LSM1-RFP* was proliferated at 30°C. Exponentially proliferating cells ($1x10^7$ cells/ml) were shifted to 42ºC for 20 min. Rpb6p-GFP serves as a nuclear marker. Arrows indicate nuclear co-localization of Rpb6p-GFP and Lsm1p-RFP. Note that Dcp2p-, Xrn1p-, Edc3p-, Dcp1p-, Pat1p- or Ccr4p-RFP did not accumulate in the nuclei of these cells for as long as 1 hr at 42ºC (results not shown). (**G**) Nuclear accumulation of the indicated RFP fusion proteins in starved cells is diminished in *xrn1*^{D208A} mutant strain. WT and mutant cells were treated as in (A). Shown is the percentage of cells with nuclear RFP fusion proteins. Mean values ±SD are shown (N >150). The differences between WT and *xrn1*^{D208A} cells are statistically significant (* indicates $p<10^{-4}$). Nuclear accumulation of Xrn1p-RFP, Edc3p-RFP, Lsm1p-RFP and Dhh1p-GFP was not detected in sated or starved yMC458 or yMC461 cells under conditions used here, although nuclear accumulation of these proteins was detected in other strains.

Fig. S5, related to Fig. 5: Factors of the major mRNA decay pathway associate with chromatin of transcriptionally active genes and can stimulate transcription upon recruitment to reporter promoters. (**A**) Xrn1p-TAP associates with the indicated amplicons. (**B**) The indicated DFs associate with the *TEF4* promoter. Results of qPCR

were expressed as fold enrichment relative to the signal of No-TAP control. Mean values, normalized to the input signal and an internal *lacZ* spike (see Experimental procedures), ±SD are shown. Amplicon names represent the middle nucleotide of the amplicons relative to the translation start site. (**C**) RNase treatment does not reduce ChIP signal of Xrn1p-TAP and Dcp2p-TAP. (**D**) ChIP signal of Dcp2p-TAP is reduced in strain *xrn1*^{D208A}. Shown for eachof the indicated ampliconsis the % of the signal of yMC520 (*xrn1*^{D208A}) from yMC519 (WT). (**E**) Levels of β-gal activity expressed in Miller units in strains shown in Fig. 5E. Average of at least three experiments (± SD) are shown. * $p \leq 0.05$ compared to vector (Gal4p-BD) alone. (**F**) Northern blot analysis of *GAL4*-BD fusion genes. The same membrane in Fig. 5E was probed against *GAL4*-BD. (**G**) Western blot images of the Gal4p-BD fusion proteins. The levels of the various mRNAs were comparable, except for those encoding *XRN1*, *xrn1*^{D208A}, *PAT1* and *dcp2-4* (F). Western analysis (G) did not show any clear correlation between protein level and (in)ability to activate transcription. Nevertheless, it is clear that the inability to activate transcription of at least three of our negative controls, as well as Gal4p-BD-Edc3p and Gal4p-BD-Dcp1p was not due to low protein levels, since these levels were higher than the positive control, Gal4p-BD-Rpb3p, that strongly activates transcription. Moreover, the levels of Gal4p-BD-Dcp2p, and Gal4p-BD-Dhh1p that activate transcription were lower than that of the negative control Gal4p-BD. It is possible that the inability of Gal4p-BD-Xrn1p or Gal4p-BD-Xrn1^{D208A}p to activate transcription was due to its poor expression. Alternatively, Xrn1p might function only in elongation, as suggested by the results described in the next section.

Fig. S6, related to Fig. 6: Factors of the major mRNA decay pathway affect transcription elongation. (A) Run-on signal at the indicated positions along *GAL1* in cells grown in galactose medium. Data are expressed relative to the 5´ position for each strain, followed by normalization of each value to the corresponding position in the wild type, which was defined as "1". Mean values and SD of three independent experiments are shown. (**B**) Northern blot image (left panel) and quantification by phosphor imager (right panel) using probes for the indicated mRNAs of WT or Δ*dst1* cells expressing different Gal4p-BD fusion proteins.* - exposure time is 6-fold of that shown in the upper image. (**C**) mRNA Decay mutants are sensitive to the drug 6-azauracil (6-AU). The indicated strains (WT is yMC370) were spotted in a five-fold serial dilution (the first spot is $1x10^5$ cells) on 6-AU or control plates as described in Experimental procedures. The photo was taken after two days of proliferation at 28°C.

Supplementary Movies

Movies S1 to S4, related to Fig. 3: Three-dimensional (3D) reconstruction of FISH images clearly distinguishes between cytoplasmic and nuclear mRNAs.

3D reconstructions of FISH analysis of *TEF4* mRNA (green spots) and the cell nucleus stained by DAPI (blue area) were performed as described in the Extended Experimental procedures. Movies S1, S2 and S3 show examples of a WT cell, a Δ*xrn1* cell and an

xrn1^{D208A} cell, respectively, each containing a single *TEF4* mRNA spot in the nucleus. Movie S4 shows an example of an *xrn1*^{D208A} cell with no mRNA spot in the nucleus, i.e. no TS.

(Please click on the link on pages 96 -99 to download the movie files).

Supplementary Tables

Table S1, related to Fig 1: mRNA levels vs half-lives
A list of three hundred mRNAs whose stability was severely increased by deletion of *XRN1,* but their steady-state levels were little perturbed**. (Please click on the link on page 93 to download the Excel file).**

Table S2, related to Fig. 1: calculated transcription rates.

Mutant	Gene	RA (SS level)[a]	Relative RS[a]	Calculated TR[b]
Δxrn1	*RPS28B*	3.0	13.3	0.23
	RPL25	0.96	3.6	0.27
	ACT1	0.39	1.7	0.24
	YEF3	0.56	1.5	0.37
	RPL43A	1.2	1.6	0.74
	TEF4	1.3	2.0	0.65
	PMA1	1.6	1.8	0.89
	RPL30	1.3	2.4	0.54
	NSR1	1.7	3.6	0.47
	EDC1[c]	17.0	22.5	0.76
Δdhh1	*RPS28B*	0.75	1.3	0.56
	RPL25	0.49	1.0	0.49
	ACT1	0.33	2.4	0.14
	YEF3	0.36	1.9	0.19
	RPL43A	0.65	2.4	0.27
	TEF4	0.76	1.7	0.44
	RPL30	0.63	3.0	0.21
	NSR1	0.69	2.6	0.27
	EDC1[c]	5.0	22.5	0.22
Δpat1	*RPS28B*	0.83	1.5	0.55
	RPL25	1.2	3.0	0.40

	ACT1	0.77	2.2	0.35
	YEF3	0.67	2.2	0.31
	RPL43A	0.81	2.4	0.33
	TEF4	0.84	2.5	0.34
	PMA1	1.0	2.0	0.50
	RPL30	0.87	3.0	0.29
	NSR1	0.69	2.2	0.31
	EDC1[c]	2.7	22.5	0.12

[a] – RA (steady state) and Relative stability (RS) levels are shown as fold of WT. RS is calculated as the half-life in the mutant divided by half-life in WT.
[b] - Transcription rate (TR) is calculated as RA/RS. The result is the relative TR compared to WT.
[c] - Data for *EDC1* mRNA was taken from (Muhlrad and Parker, 2005).

Table S3, related to Fig S1: **Physical and Genetic interactions between decay factors and factors involved in the nuclear stages of gene expression**. The data presented in this Excel file was collected from SGD (http://www.yeastgenome.org). The superscripted numbers next to each gene or protein name relate to the reference list in the second spreadsheet. Genetic interactions are depicted as gene names; physical interactions are depicted as protein names. This table is summarized in Fig. S1B.

(Please click on the link on page 94 to download the Excel file).

Table S4, related to Figs. 1 and 7: Detailed TR, RA, HL and DR results. Detailed transcription (TR), mRNA steady state amount (RA) and mRNA half-life (HL) and mRNA decay rate (DR) data for each gene in the GRO macroarray and thiolutin shut-off assay in the two mutant strains relative to WT cells in each of the DR categories: "strong decrease" and "moderate decrease" (see legend to Fig. 7A). Note that the Excel file contains four sheets with different data sets.

(Please click on the link on page 95 to download the Excel file).

Table S5, related to Fig 5: Proliferation of yeast cells expressing tethered DFs on 3-Amino-2,3-Triazole (3-AT) plates.

GAL4-BD fusion	3-AT threshold (mM)[a]	Comments
RPB3	100	Positive control
GAL4-BD	(-)	Negative control
HSP104	(-)	Non-DF control
TOR1	(-)	Non-DF control
RAD17	(-)	Non-DF control
ELG1	(-)	Non-DF control
DOT1	(-)	Non-DF control
EDC3	(-)	
XRN1	(-)	
xrn1^{D208A}	0	
DCP1	0	
LSM1	1	
CCR4	5	
DCP2	20	
dcp2-4	100	
DHH1	100	
PAT1	200	

[a] The maximal 3-AT concentration (in mM) that allowed proliferation on SC-Trp-His plate during 4-day incubation at 30ºC. Note that the Gal4p-BD fusion protein drives expression of *HIS3*, whose expression level is assayed here.

(-) – no growth on SC-Trp-His even at 0 mM 3-AT level.

Table S6, related to Fig 1 and S1: data of RNA levels for macroarray analysis.

	(mRNA / total RNA) [a]	(total RNA / cell)[b]	(mRNA / cell)
YMC458 (WT)	1	1	1
YMC461 (*xrn1*^{D208A})	1.194	0.92	1.1
YMC511 (Δ*xrn1*)	0.996	0.82	0.82

[a] Experion^{TM} data.

[b] Coulter counter and total RNA purification data.

All numbers are relative to WT data. See GRO section in Extended experimental

procedures for more details.

Extended Experimental procedures

Yeast strains and plasmids

Yeast strains and plasmids are listed in the tables below. To construct yMC609 and yMC662, the Δ*xrn1*::*KanMX4* cassette from yMC362 was PCR amplified and subsequently introduced into the chromosome by genomic replacement and selecting on YPD-G418 plates. Similarly, strains yMC412 and yMC757 were constructed with PCR amplified Δ*pat1::KanMX4* and Δ*dst1::KanMX4* cassettes from yMC363 and yMC471, respectively. Strain yMC399 was constructed with plasmid pMC349. To construct yMC571, the TAP-*TRP1* cassette from pMC281 (Puig et al., 2001) was PCR amplified and subsequently introduced into the chromosome by genomic replacement and selecting on SC-Trp plates. To construct yMC519 and yMC520, the *DCP2*-TAP cassette from yMC454 was PCR amplified and subsequently introduced into the chromosome of yMC458 and yMC461, respectively, by genomic replacement and selecting on SC-Ura plates. yMC422, yMC426 and yMC511 were created by selecting 5-FOA resistant clones of yMC420, yMC371 and yMC459, respectively.

Plasmids pMC353, pMC438, pMC439, pMC440, pMC466 and pMC467 were created by replacing the *LSM1* gene in pMC270 with PCR fragments containing the corresponding gene with its native promoter (~500bp upstream to the ATG) by *in vivo* recombination. Plasmids pMC391 and pMC449 were created by replacing the *URA3* marker on pMC350 and pMC269, respectively, with the *ADE2* marker of pMC388 by *in vivo* recombination. pMC476 was created by replacing the *DHH1*-GFP from pMC391 with a PCR amplified

fragment containing *PAB1*-GFP with its native promoter (427bp upstream to ATG), from yMC497, by *in vivo* recombination. Plasmids pMC491 and pMC492 were created by digesting pMC466 and pMC467, respectively, with BamHI and XbaI to extract the RFP sequence. The GFP was inserted in frame by *in vivo* homologous recombination with a PCR amplified *XRN1*-GFP fragment from yMC499. *XRN1* mutants R101G, D208A,R101G and H41D were created as follows: pMC491, pMC492, pMC560, pMC558 and pMC467 were double digested with SpeI and AgeI. The 2545bp SpeI-AgeI fragment from pMC467 and pMC560 was further digested with SfaNI (1/4 of the SpeI-AgeI fragment of pMC560 was kept un-digested). To get pMC580 and pMC582, pMC491 was ligated with the SpeI-AgeI fragment of pMC558 and pMC560, respectively. To get pMC579, pMC492 was ligated with the AgeI-SfaNI fragment of pMC560 and SfaNI-SpeI fragment of pMC467. The correct sequence of the new mutants was verified by sequencing.

Plasmids for expression of Gal4p-BD-DFs fusion proteins (pGHOTHY plasmids) were constructed according to the instructions of Yeast Resource Center (YRC, University of Washington).

Yeast strains

Name	**Genotype**	**Source**
yMC229	*MATa, his3Δ1, leu2Δ0, met15Δ0, ura3Δ0,*	EUROSCARF (BY4741)
yMC323	*MATa his3Δ1 leu2Δ0 met15Δ0 ura3Δ0 rpb4::KanMX4*	EUROSCARF
yMC362	*MATa, his3Δ1, leu2Δ0, met15Δ0, ura3Δ0, xrn1::KanMX4*	EUROSCARF
yMC363	*MATa, his3Δ1, leu2Δ0, met15Δ0, ura3Δ0, pat1::KanMX4*	EUROSCARF
yMC364	*MATa, his3Δ1, leu2Δ0, met15Δ0, ura3Δ0, lsm1::KanMX4*	EUROSCARF

yMC404	*MATa, his3Δ1, leu2Δ0, met15Δ0, ura3Δ0, dhh1::KanMX4*	EUROSCARF
yMC429	*MATa, his3Δ1, leu2Δ0, met15Δ0, ura3Δ0, edc3::KanMX4*	EUROSCARF
yMC470	*MATa, his3Δ1, leu2Δ0, met15Δ0, ura3Δ0, ccr4::KanMX4*	EUROSCARF
yMC471	*MATa, his3Δ1, leu2Δ0, met15Δ0, ura3Δ0, dst1::KanMX4*	EUROSCARF
yMC370	*MATα, leu2-3,112 lys2-201 trp1, His4-539, ura3-52, cup1::LEU2/PGK1pG/MFA2pG*	Gift of R. Parker (yRP841)
yMC372	*MATα, leu2-3,112 lys2-201 trp1, His4-539, ura3-52, cup1::LEU2/PGK1pG/MFA2pG, lsm1::TRP1*	Gift of R. Parker (yRP1739)
yMC419	*MATα, leu2-3,112 lys2-201 trp1, His4-539 ura3-52 cup1::LEU2/PGK1pG/MFA2pG ccr4Δ::NEO, pan2Δ::URA3*	Gift of R. Parker (yRP1620)
yMC420	*MATα, leu2-3,112 lys2-201 trp1, His4-539, ura3-52, cup1::LEU2/PGK1pG/MFA2pG, dcp1::URA3*	Gift of R. Parker (yRP1200)
yMC422	*MATα, leu2-3,112 lys2-201 trp1, his4-539, ura3-52, cup1::LEU2/PGK1pG/MFA2pG, dcp1::ura3*	This work
yMC374	*MATα, leu2-3,112 lys2-201 trp1, His4-539 ura3-52 cup1::LEU2/PGK1pG/MFA2pG, dcp2::TRP1*	Gift of R. Parker (yRP1358)
yGH177	*MATα, leu2-3,112 lys2-201 trp1, His4-539, ura3-52, cup1::LEU2/PGK1pG/MFA2pG, dcp2::TRP1, [pMC406 (URA3 CEN) dcp2-4]*	This work
yMC371	*MATα, leu2-3,112 lys2-201 trp1, His4-539, ura3-52, cup1::LEU2/PGK1pG/MFA2pG xrn1::URA3, DHH1-GFP (NEO)*	Gift of R. Parker (yRP1738)
yMC426	*MATα, leu2-3,112 lys2-201 trp1, His4-539, ura3-52, cup1::LEU2/PGK1pG/MFA2pG xrn1::ura3, DHH1-GFP (NEO)*	This work
yMC375	*MATa, ura3, his3, leu2*	Gift of R. Parker (yRP2065)
yMC399	*MATa, ura3, his3, leu2, Δdhh1::LEU2*	This work
yMC412	*MATa, ura3, his3, leu2, Δpat1::KanMX4*	This work
yMC376	*MATa, ura3, his3, leu2, dhh1::NEO, pat1::NEO*	Gift of R. Parker (yRP2069)
yMC458	*MATa, ade2, ura3-52, XRN1*	Gift of WD Heyer (WDHY548)
yMC459	*MATa, ade2, ura3-52, xrn1::URA3*	Gift of WD Heyer (WDHY448)
yMC461	*MATa, ade2, ura3-52, xrn1^{D208A}*	Gift of WD Heyer (WDHY493)
yMC511	*MATa, ade2, ura3-52, xrn1::ura3*	This work
yMC566	*MATa, ade2, his3 ,leu2, trp1, ura3,*	Gift of K. Weis (KWY171)

	mex67::HIS3 [pUN100 (CEN LEU2) MEX67]	
yMC568	*MATa, ade2, his3, leu2, trp1, ura3, mex67::HIS3 [pUN100 (CEN LEU2) mex67-5], xpo1::TRP1, xpo1-1::HIS3*	Gift of K. Weis (KWY610)
yMC609	*MATa, ade2, his3, leu2, trp1, ura3, mex67::HIS3 [pUN100 (CEN LEU2) mex67-5], xpo1::TRP1, xpo1-1::HIS3 Δxrn1::KanMX4*	This work
yMC495	*MATa, ade2, arg4, leu2-3,112, trp1-289, ura3-52*	EUROSCARF
yMC593	*MATa, ade2, arg4, leu2-3,112, trp1-289, ura3-52, RPB3::TAP-K.I URA3*	EUROSCARF
yMC453	*MATa, ade2, arg4, leu2-3,112, trp1-289, ura3-52, XRN1::TAP-K.I URA3*	EUROSCARF
yMC454	*MATa, ade2, arg4, leu2-3,112, trp1-289, ura3-52, DCP2::TAP-K.I URA3*	EUROSCARF
yMC278	*MATa, ade2, arg4, leu2-3,112, trp1-289, ura3-52, LSM1::TAP-K.I URA3*	EUROSCARF
yMC514	*MATa, ade2, arg4, leu2-3,112, trp1-289, ura3-52, CCR4::TAP-K.I URA3*	EUROSCARF
yMC571	*MATa, ade2, arg4, leu2-3,112, trp1-289, ura3-52, DHH1::TAP-TRP1*	This work
yMC581	*MATa, ade2, arg4, leu2-3,112, trp1-289, ura3-52, PAT1::TAP-K.I URA3*	EUROSCARF
yMC582	*MATa, ade2, arg4, leu2-3,112, trp1-289, ura3-52, DCP1::TAP-K.I URA3*	EUROSCARF
yMC519	*MATa ade2 ura3-52 XRN1 DCP2-TAP-K.I. URA3*	This work
yMC520	*MATa ade2 ura3-52 xrn1*^{D208A} *DCP2-TAP-K.I. URA3*	This work
yMC497	*MATa, his3Δ1, leu2Δ0, met15Δ0, ura3Δ0, PAB1-GFP-HIS3X6*	Invitrogen
yMC499	*MATa, his3Δ1, leu2Δ0, met15Δ0, ura3Δ0, XRN1-GFP-HIS3X6*	Invitrogen
yMC334	*MATa, his3Δ1, leu2Δ0, met15Δ0, ura3Δ0, RPB6-GFP-HIS3X6*	Invitrogen
yMC646	*MATα trp1-901, leu2-3,112, ura3-52, his3-200, Δgal4, Δgal80, LYS2::*P_{GAL1}*-HIS3,* P_{GAL2}*-ADE2, met2::*P_{GAL7}*-lacZ*	YRC (PJ69-4α)
yMC662	*MATα trp1-901, leu2-3,112, ura3-52, his3-200, Δgal4, Δgal80, LYS2::*P_{GAL1}*-HIS3,* P_{GAL2}*-ADE2, met2::*P_{GAL7}*-lacZ Δxrn1::KanMX4*	This work
yGH424	*MATα trp1-901, leu2-3,112, ura3-52, his3-200, Δgal4, Δgal80, LYS2::*P_{GAL1}*-HIS3,* P_{GAL2}*-ADE2, met2::*P_{GAL7}*-lacZ Δxrn1::KanMX4 [pMC467(CEN, URA3) xrn1*^{D208A}*-RFP]*	This work

yMC757	*MATα trp1-901, leu2-3,112, ura3-52, his3-200, Δgal4, Δgal80, LYS2::P_{GAL1}-HIS3, P_{GAL2}-ADE2, met2::P_{GAL7}-lacZ Δdst1::KanMX4*	This work

Plasmids

Plasmid	**Description**	**Source**
pMC349	*Δdhh1::LEU2*	Gift of TH Chang
pMC388	*ura3::ADE2*	Gift of D. Kornitzer
pMC406	*dcp2-4/URA3/CEN*	Gift of R. Parker
pMC269	*DCP2-RFP/URA3/CEN*	Gift of R. Parker
pMC270	*LSM1-RFP/URA3/CEN*	Gift of R. Parker
pMC468	*LSM1-mCh/LEU3/CEN*	Gift of R. Parker
pMC350	*DHH1-GFP/URA3/CEN*	Gift of TH Chang
pMC353	*PAT1-RFP/URA3/CEN*	This work
pMC391	*DHH1-GFP/ADE2/CEN*	This work
pMC438	*EDC3-RFP/URA3/CEN*	This work
pMC439	*DCP1-RFP/URA3/CEN*	This work
pMC440	*CCR4-RFP/URA3/CEN*	This work
pMC476	*PAB1-GFP/ADE2/CEN*	This work
pMC466	*XRN1-RFP/URA3/CEN*	This work
pMC467	*xrn1^{D208A}-RFP/URA3/CEN*	This work
pMC344	*RPB4-GFP/HIS3/CEN*	This work
pMC491	*XRN1-GFP/URA3/CEN*	This work
pMC492	*xrn1^{D208A}-GFP/URA3/CEN*	This work
pMC558	*xrn1^{H41D}/LEU2/CEN*	Gift of A. Johnson
pMC560	*xrn1^{R101G}/LEU2/CEN*	Gift of A. Johnson
pMC579	*xrn1^{D208A,R101G} -GFP/URA3/CEN*	This work
pMC580	*xrn1^{H41D}-GFP/URA3/CEN*	This work
pMC582	*xrn1^{R101G} -GFP/URA3/CEN*	This work
pMC449	*DCP2-RFP/ADE2/CEN*	This work
pMC281	*TAP-TRP1*	EUROSCARF (pBS1479)
pMC293	*GAL4-BD/TRP1/CEN*	YRC (pOBD2)
pNOTHY10	*GAL4-BD-HSP104/TRP1/CEN*	YRC
pNOTHY76	*GAL4-BD-TOR1/TRP1/CEN*	YRC
pGHOTHY35	*GAL4-BD-RPB3/TRP1/CEN*	This work
pGHOTHY36	*GAL4-BD-LSM1/TRP1/CEN*	This work
pGHOTHY38	*GAL4-BD-XRN1/TRP1/CEN*	This work
pGHOTHY42	*GAL4-BD-xrn1^{D208A}/TRP1/CEN*	This work

pGHOTHY43	*GAL4-BD-DCP1/TRP1/CEN*	This work
pGHOTHY44	*GAL4-BD-DCP2/TRP1/CEN*	This work
pGHOTHY46	*GAL4-BD-DHH1/TRP1/CEN*	This work
pGHOTHY47	*GAL4-BD-EDC3/TRP1/CEN*	This work
pGHOTHY49	*GAL4-BD-CCR4/TRP1/CEN*	This work
pGHOTHY50	*GAL4-BD-PAT1/TRP1/CEN*	This work
pGHOTHY54	*GAL4-BD-dcp2-4/TRP1/CEN*	This work
pGHOTHY261	*GAL4-BD-RAD17/TRP1/CEN*	Gift of S. Ben Aroya
pGHOTHY262	*GAL4-BD-DOT1/TRP1/CEN*	Gift of S. Ben Aroya
pGHOTHY263	*GAL4-BD-ELG1/TRP1/CEN*	Gift of S. Ben Aroya

Yeast proliferation.

Yeast cells were proliferated in synthetic complete medium (SC) at 30°C unless otherwise indicated. Cells were maintained for at least seven generations at the exponential growth phase prior to harvesting. For starvation experiments, cells were washed once with water and then resuspended in SC lacking both carbon source and amino acids. For nucleo-cytoplasmic shuttling experiments, cells were allowed to proliferate at 24ºC to 3-5x10^6 cells/ml and subsequently incubated for 1-2 h at 37°C as indicated in the figure legend. Cycloheximide (Sigma) was added to a final concentration of 100 µg/ml just prior to temperature shift.

Proliferation on 6-azauracil (6-AU) plates

Plate preparation: stock solution of 50 mg/ml 6-AU (Sigma) was prepared in 1M NH_4OH and diluted to 100µg/ml in SC-ura just prior to pouring the plates. Control plates were prepared by addition of the same volume of 1M NH_4OH just prior to pouring, to eliminate any effect of changes in pH on proliferation. Cells were serially diluted 1:5,

spotted on the plates (first spot is equivalent to $1x10^5$ cells) and incubated for 2 days at 28°C prior to photography.

Proliferation on 3-Amino-2,3-Triazole (3-AT) plates

SC plates lacking both Tryptophan and Histidine and containing either 0, 1, 3, 5, 10, 20, 50, 100 or 200 mM of 3-Amino-2,3-Triazole (3-AT; Sigma) (Titz et al., 2006) , or plates lacking only Tryptophan (as a positive control for proliferation) were prepared. Proliferation on the plates was determined by streaking the cells on the plates and assessing growth after four days at 28°C. The cells are more resistant to 3-AT the higher they express His3p. Cells which do not express His3p at all will not be able to grow on plates lacking Histidine, even at 0 mM 3-AT.

Determining mRNA steady state levels (RA) and stability; transcriptional induction and repression.

For determining steady-state levels of mRNAs (RA), cells were harvested at $1x10^7$ cells/ml. For the galactose-glucose experiments, cells were grown to $1x10^7$ cells/ml in SC containing 2% raffinose instead of glucose. The sample of time point "0" was taken just prior to galactose addition. Galactose was added to a final concentration of 2% (SC-Raf/Gal) and samples were collected at the indicated times. After 75 min incubation in SC-Raf/Gal, the remaining cells were washed twice with water at room-temperature and then resuspended in pre-heated (30°C) SC containing 4% glucose and samples were collected at the indicated time points thereafter. For the heat-shock experiments, optimally proliferating cells (200 ml of $1x10^7$cells/ml) were shifted rapidly from 30°C to 42°C by shaking for 50 seconds at 70°C and then incubated at 42°C for 30 min. This

treatment leads to induction of HS genes and transcriptional arrest of most genes, including those encoding protein biosynthetic factors (PBF; e.g. *TEF4* and *RPL43A*(Lotan et al., 2005; Lotan et al., 2007)). After 30 min incubation at 42°C, cultures were rapidly cooled in ice-water slurry (35 seconds) back to 30°C, which leads to transcription induction of PBF genes, and transcriptional arrest of HS genes. Samples were collected at the indicated times. To assess mRNA stability at 30°C, 1-10 phenanthroline (Merck) was added to a final concentration of 100 µg/ml (Grigull et al., 2004). The thiolutin shut-off assay was performed as described previously (Pelechano and Perez-Ortin, 2008). Thiolutin (Pfizer) was added to 5 µg/ml to YPD cultures at 28ºC.

Northern blot analysis.

Samples for Northern blot were collected as follows: 25ml of culture was fast cooled to 4°C in liquid N_2. Samples were then centrifuged at maximum speed at 4°C for 2 min and the cell pellet was washed once with 1 ml ice-cold water, then frozen in liquid N_2 and stored at -80°C until used. RNA extraction and Northern blot analysis were performed as previously described (Lotan et al., 2005).

Fluorescent in situ hybridization (FISH)

Probes: FISH probes approximately 50 bp long were designed and checked for specificity. Five thymidine bases per probe were amine-modified (Eurogentec, 6C-Amino dT). These were then labeled using commercial amine mono reactive Cy3 or Cy5 dyes (Amersham, PA23001 and PA25001, respectively) to a labeling efficiency greater than 80%. Amino allyl modified Cy3 and Cy5 labeled thymidines are marked by an asterisk on the following probe sequences:

T*CAACATATGAGAGGT*TACCTATTAT*TACCCATT*CAGACA GGGATAACT*G	snR38_1
T*ACCCAAAAAT*GCAGGGGCTT*GCTTCAAT*GGGAACAAAG AAGCAAACT*CGC	YKL081W_1
T*GGACGAGCAAT*GTTGCTCATGACAT*CGGAATTAGCT*AG AGATGCCCAT*C	YKL081W_2
T*CGGTAGCAACAAAGGT*GTAGTCTCT*CAATCTAGCAT*CG AAGACAGCAGCT*A	YKL081W_3
T*GTTGAACCAT*CTCATCAAAT*GAGGATGCTT*AGCTCTCCA TT*CAGGGCCC	YKL081W_4
T*CGGCCTTTGGCT*TTTCAGCCTT*TTGCTTCTTT*GGTGGAGT GTAGGTT*AG	YKL081W_5

Proliferation, fixation and hybridization: WT (yMC458), Δ*xrn1* (yMC459) and *xrn1*^{D208A} (yMC461) strains were proliferated at 30°C in YPD medium to an optical density at 600nm of 0.8. Cells were fixed by incubation in 4% (v/v) paraformaldehyde in YPD, at room temperature for 45 min. Cells were spheroplasted using lyticase (Sigma-Aldrich L2524) and deposited on cover slips coated with poly-L-Lysine (Sigma-Aldrich P8920). The cover slips were then stored at -20°C in 70% (v/v) ethanol. Prior to hybridization, the cover slips were washed twice in PBS for 10 min for rehydration, incubated for 15 min in PBS supplemented with 0.5% Triton for membrane permeabilization, then equilibrated with hybridization buffer by incubating once in PBS for 10 min and twice in 2x SSC, 40% (v/v) formamide for 5 min. Cover slips were hybridized against 1 ng of fluorescently labeled DNA probes, 5 µg of salmon sperm DNA and 5 µg of E.coli tRNA, in 20 µl of a solution at 5 mM Na_2HPO_4, 40% (v/v) formamide, 2x SSC, 2 mg/ml BSA, 10 mM VRC, 0.12 U/µl RNase inhibitor.

Hybridization was done overnight at 37°C. Cover slips were rinsed twice in 2x SSC, 40% (v/v) formamide at 37°C for 15 min, then twice in PBS for 1 h, at room temperature. They were stained with 0.5µg/ml DAPI in PBS and mounted in 90% glycerol in PBS (pH=8.5) containing 1 mg/ml P-phenylenediamine (Sigma-Aldrich 695106).

Image acquisition: Images were acquired with a Nikon Eclipse Ti, using a plan Apochromatic x100 oil immersion objective with a 1.4 numerical aperture. A Nikon Intensilight C-HGFI lamp was used to illuminate the cover slips. Dichroic filters for Cy3 (Semrock Cy3-4040B), Cy5 (Semrock Cy5-4040A) and DAPI (Semrock DAPI-1160A) were used. Stacks of 41 images were acquired in z-steps of 0.2 µm using a Photometrics Coolsnap HQ² camera.

Data analysis: Images were analyzed z-step by z-step by an IPlab IDL virtual machine program which uses a 2D Gaussian fit algorithm to detect FISH spots and to extract integrated intensity, as previously described (Thompson et al., 2002; Zenklusen et al., 2008). Spots detected over several continuous planes were treated as a single object and the value corresponding to the focal plane (maximal intensity) was used for analysis. Only the integrated intensities at the focal point were used for statistical analysis. These intensities were normalized to their median. 209 cells were analyzed for the WT strain, 76 for the Δ*xrn1* strain and 240 for the *xrn1*^{D208A} strain.

Three dimensional (3D) reconstructions: The 3D reconstructions of the cells were made by extracting the x, y, and z coordinates calculated by 2D Gaussian fitting. The highest integrated intensity of the spot was chosen for the plane of the z coordinate. The coordinates of the threshold DAPI signal were also extracted. These coordinates were corrected for the true voxel size (43nm in the x and y directions, 200 nm in the z

direction), therefore obtaining the coordinates in nanometers. These coordinates were imported in Mathematica (Wolfram research, inc. Champaign, Illinois, USA), and were plotted in a 3D environment after smoothing and hollowing of the nucleus volume. 75 images were taken by rotating the viewpoint around the y axis in regular steps of $2\pi/75$.

Statistical analysis: Because the distribution law of transcription site intensities is unknown, we used a bootstrapping resampling method (Simon, 1997) to evaluate variability for each histogram bin in the FISH assay. Error bars in histograms represent the 2.5^{th} and 97.5^{th} percentiles of each resampled bin (Bootstrapping depth was 10,000). P values used to evaluate the differences between histograms of two different strains were also obtained by resampling. The two original populations were pooled and resampled iteratively into two populations. Histograms from the resampled populations were subtracted at each iteration giving a range of differences for each histogram bin. The P value represents the probability to obtain a difference greater or equal to the observed difference by resampling.

Genomic run-on (GRO)

For the whole genome GRO, mRNA amounts (RA) were normalized using the median of Pol II spots and corrected by the concentration of total mRNA/cell. mRNA concentration in each of the three strains, WT and the two *xrn1* mutants, was obtained from the data of total RNA/cell (three independent samples of known cell number) and cell median volumes (obtained by Coulter counter). The proportion of mRNA in total RNA was calculated from the electropherograms of total RNA obtained in an Experion^{TM} device as the percentage of area in between the 5S and 18S rRNA peaks with regard to the total

area (see Table S6). Transcription rates (TR) of Pol II transcripts were averaged between the three replicates. Reassuringly, the GRO data and FISH data, both determining the relative number of elongating Pol II in *TEF4*, were consistent with each other. There was also a good agreement between the GRO and steady-state mRNA levels shown in Fig. S1A (strain 4).

3'/5' ratio analysis and RNA pol II ChIP on chip (RPCC) experiments.

Specialized nylon macroarrays containing 300 bp probes obtained by PCR amplification for 384 selected yeast genes were previously described (Rodriguez-Gil et al., 2010). They were used with run-on samples obtained as described above but with an additional step of RNA fragmentation with 40 mM NaOH for 5 min as described (Rodriguez-Gil et al., 2010), for the determination of elongating Pol II molecules. The same arrays were re-probed with labeled DNA from ChIP of identical yeast samples immunoprecipitated with the 8WG16 RNA pol II antibody (RPCC, RNA pol II ChIP on chip) as previously described (Pelechano et al., 2009; Rodriguez-Gil et al., 2010) for the determination of total Pol II molecules. Two independent replicates for both kinds of experiments were done. Only genes with valid data (over 1.3 times over background) in two replicates were considered and averaged using a median absolute deviation protocol to filter outliers. 3'/5' ratios for each gene were calculated for those genes which had valid data in both 3' and 5' probes. 268 genes for WT, 211 genes for *Δxrn1* and 64 genes for *xrn1*^{D208A} strains gave valid data in GRO experiments and 316 genes for WT, 332 genes for *Δxrn1* and 362 genes for *xrn1*^{D208A} strains gave valid data in RPCC experiments. These values were used for comparing mutant vs. WT ratios when possible. A Wilcoxon signed rank test was applied to check the significance of the differences found between WT and mutant strains

data.

Chromatin Immuno-precipitation (ChIP) with TAP tagged proteins

Cell cultures (200 ml) were harvested at 1.5-2x10^7 cells/ml. Cross linking was done by adding formaldehyde to a final concentration of 0.75% to the cell culture (this gave us better results than using 1%) and incubating at room temperature for 20 min with mild shaking. Quenching was done by adding glycine to a final concentration of 125 mM and incubating at room temperature for 5 min with mild shaking. Cells were then washed once with cold TBS (20 mM Tris-HCl pH=7.4, 150 mM NaCl) and the cell pellet was either used immediately or stored at -80°C. To lyse the cells, 700 µl of lysis buffer (50 mM HEPES-KOH pH=7.5, 300 mM NaCl, 1 mM EDTA, 1% Triton X-100, 0.1% sodium deoxycholate supplemented with the following protease inhibitors: Complete protease inhibitor cocktail (Roche) 1 tablet/25 ml, PMSF 2 mM, TLCK 50 µg/ml and benzamidine 2.5 mM) was added to the frozen cell pellet. The tube was filled with 0.5 mm acid-washed glass beads and lysis was done by 5 cycles of alternating between 1 min of beating (50 rpm) in a Mini-Bead Beater (Biospec Products, Bartlesville, OK) and 1 min on ice. The lysate was sonicated 3x10 sec at level 10 with Microson sonicator (Misonix, Inc., Farmingdale, NY) or 25 cycles of 30 sec/50 sec on/off, level set to high (Bioraptor, Diagenode, Belgium) and cleared by two rounds of centrifugation. Average DNA fragment size was ~500 bp. In experiments where RNase was added, the lysate was pre-treated for 30 min at room temperature with 15µl RNase cocktail (RNase A at 500 U/mL; RNase T1 at 20,000 U/mL; Ambion). The RNases continued to be present

thereafter in the next steps. Protein samples (1.5mg) were loaded onto 50 µl IgG Sepharose beads (6 Fast Flow) (GE Healthcare Bio-Sciences) which had been blocked for 1 h with 1 mg/ml of BSA, and incubated at 4°C with mild rotation for 1 h. IgG beads were washed three times with lysis buffer, twice with WASH 2 buffer (50 mM HEPES-KOH pH=7.5, 500 mM NaCl, 1 mM EDTA, 1% Triton X-100, 0.1% sodium deoxycholate supplemented with the protease inhibitors mentioned above), three times with WASH 3 buffer (10 mM Tris-HCl pH=8.0, 250 mM LiCl, 2 mM EDTA, 1% Triton X-100, 0.1% sodium deoxycholate supplemented with the protease inhibitors mentioned above) and twice with TE (10 mM Tris-HCl pH=8.0, 1 mM EDTA). Two different elution protocols were used, TEV-mediated and SDS-mediated elution. The strain harboring *RPB3*-TAP and the No-TAP strain were subjected to both elution protocols. For Xrn1p-TAP, the TEV-mediated elution worked better. For all other TAP-tagged proteins both methods worked well. TEV mediated elution: beads were washed twice with TEV buffer (10 mM Tris-HCl pH=8.0; 150 mM NaCl; 0.1% NP-40; 0.5 mM EDTA; 1 mM DTT) and then resuspended in 200 µl TEV buffer. Elution was done by adding 10 U of AcTEV protease (Invitrogen) and incubation at 24°C for 3.5 h with mild rotation. For all other TAP-tagged proteins, 150 µl of SDS elution buffer (10 mM Tris-HCl pH=8.0, 10 mM EDTA, 1% SDS) was added to the beads and samples were incubated for 30 min at 65°C. In both cases, elution buffer was spiked with an exogenous *lacZ* DNA fragment which was later used to determine recovery during subsequent stages. Following TEV cleavage or SDS elution, samples were centrifuged at 2000 rpm for 1 min and the supernatant was transferred to Spin-X centrifuge tube filters (Costar). The beads were washed with 70 µl TEV buffer or 100 µl SDS elution buffer and the

supernatant was combined. Samples were filtered in Spin-X tube to filter out any possible contamination of beads in the eluted material. De-cross-linking was done by incubation overnight at 65°C. To purify the DNA, an equal volume of TE buffer (Tris-HCl pH=7.4, 1 mM EDTA) containing 1% SDS and 200 µg/ml of proteinase K (Pierce) was added and samples were incubated for 2 h at 37°C, followed by phenol/chloroform extraction. The aqueous phase was supplemented with 1 µl of 20 mg/ml glycogen and the DNA was ethanol precipitated. DNA was resuspended in 60 µl of PCR grade water. Input samples (usually 10% from the sample loaded on the beads) were diluted in TEV or SDS elution buffer containing *lacZ* DNA spike and then treated identically from the de-cross-linking stage onward.

Real-time PCR (qPCR): The Absolute blue SYBR Green ROX mix (Thermo Scientific) was used for qPCR according to the manufacturer's instructions in a 10µl reaction volume. qPCR was performed in Rotor-Gene 6000 (Corbett Life Science, Sydney, Australia). qPCR was performed as follows: Hold: 95°C for 15 min; Cycling: 95°C for 2 s, 54°C for 15 s, 72°C for 20 s; Melting: 60°C to 99°C with 5 s for each step. For some primers, the cycling stage was changed to 95°C for 2 s, 60°C for 20 s. Results were analyzed with Rotor-Gene 6000 Series Software v1.7. The melting curve was used to determine the purity of the PCR products. All samples were normalized to the *lacZ* DNA which was added at the elution stage of the ChIP protocol (see above). IP samples were then normalized to Input. Results for TAP-tagged proteins are shown as fold enrichment relative to the signal obtained from the No-TAP (Fig. 5B and C and Fig. S6) or as a percentage from *PMA1* amplicon 115, which was taken arbitrarily as 100% (Fig. 5A). In

all cases, amplicon length did not exceed 250 bp, and correct length was verified by gel electrophoresis. Sequences of qPCR primers will be given upon request

Pol II and Ser-2-P ChIP

Yeast cultures (100ml) were harvested at $D.O_{600nm}$=0.5. Cell lysis was performed by 3 cycles of 30s at 5m/s in Fastprep (MP Biomedicals). The lysate was sonicated 30 minutes (30s/30s on/off) utilizing a Bioruptor sonicator (Diagenode). Protein samples were loaded onto 50µl of Pan Mouse IgG Dynabeds, which were previously incubated overnight with either anti-Rpb3 (ab81859, Abcam) or anti Ser2-P (ab5095, Abcam) specific antibody, and incubated at 4ºC with mild rotation for 1.5 hours. Elution was done at 65ºC for 20 minutes with TE buffer containing 1% of SDS. For qPCR, SYBR Premix Ex Taq (Takara) was used in a 10µl reaction volume. qPCR was performed in Lightcycler 480 II (Roche). IP samples were normalized to Input.

Acknowledgments

We thank Roy Parker, Daniel Larson and Robert Singer for critically reading the manuscript. We also thank the latter two individuals for sharing their 2D gaussian fitting algorithm. Roy Parker, Wolf Heyer, Karsten Weis, Tien-Hsien Chang, Arlen Johnson, Shay Ben-Aroya and Daniel Kornitzer were generous in sharing yeast strains and plasmids with us and the Laboratorio de Chips de DNA (S.C.S.I.E. Universitat de València) generously prepared the GRO macroarrays. This work was supported by Israel Science Foundation (1283/07) and Rappaport Foundation (to M.C), ANR JC 0118-01 and

la Ligue (to X.D), the Spanish MCINN and European Union ERDF (BFU2010-21975-C03-01) and BFU2010-21975-C03-02) to J.E.P-O. and S.C., respectively, and the Regional Valencian Government (GeneralitatValenciana –PROMETEO/2011/088) (to J.E.P-O.) and from Junta de Andalucía (grants P07-CVI02623 and P08-CVI-03508) to S.C. MICINN and Junta de Andalucía grants involve EDRF resources from the European Union. D.M. is a recipient of a Santiago Grisolía fellowship from GeneralitatValenciana. G.M.-Z. is a recipient of a FPU MICINN fellowship. The authors declare no competing financial interests.

Author contributions: G.H. and M.C. conceived the main hypothesis. G.H. constructed all strains and plasmids, and designed, performed and analysed the transcription, decay and tethering experiments by Northern and β-gal assays, localization experiments, proliferation assays and PBs analysis. S.Z.C. and X.D. designed, performed and analysed the FISH experiments. D.M. and J.E,P-O. designed, performed and analysed the GRO, RPCC and thiolutin shut-off experiments. G.H. and O.B. designed, performed and analysed the ChIP of DFs. GZM and SC contributed to design 5'/3' GRO and RPCC experiments. G.Z.M. and S.C. designed, performed and analysed the Pol II and Xrn1 ChIP of *GAL1* in glucose and galactose, and the *GAL1* run-on experiments. G.H. and M.C. wrote the manuscript. J.E,P-O. and S.C. critically read and edited the manuscript. M.C. coordinated the various approaches.

Supplementary References

Brune, C., Munchel, S.E., Fischer, N., Podtelejnikov, A.V., and Weis, K. (2005). Yeast poly(A)-binding protein Pab1 shuttles between the nucleus and the cytoplasm and functions in mRNA export. RNA *11*, 517-531.

Grigull, J., Mnaimneh, S., Pootoolal, J., Robinson, M.D., and Hughes, T.R. (2004). Genome-wide analysis of mRNA stability using transcription inhibitors and microarrays reveals posttranscriptional control of ribosome biogenesis factors. Mol Cell Biol *24*, 5534-5547.

Lotan, R., Bar-On, V.G., Harel-Sharvit, L., Duek, L., Melamed, D., and Choder, M. (2005). The RNA polymerase II subunit Rpb4p mediates decay of a specific class of mRNAs. Genes Dev *19*, 3004-3016.

Lotan, R., Goler-Baron, V., Duek, L., Haimovich, G., and Choder, M. (2007). The Rpb7p subunit of yeast RNA polymerase II plays roles in the two major cytoplasmic mRNA decay mechanisms. J Cell Biol *178*, 1133-1143.

Muhlrad, D., and Parker, R. (2005). The yeast EDC1 mRNA undergoes deadenylation-independent decapping stimulated by Not2p, Not4p, and Not5p. EMBO J *24*, 1033-1045.

Pelechano, V., Jimeno-Gonzalez, S., Rodriguez-Gil, A., Garcia-Martinez, J., Perez-Ortin, J.E., and Chavez, S. (2009). Regulon-specific control of transcription elongation across the yeast genome. PLoS Genet *5*, e1000614.

Puig, O., Caspary, F., Rigaut, G., Rutz, B., Bouveret, E., Bragado-Nilsson, E., Wilm, M., and Seraphin, B. (2001). The tandem affinity purification (TAP) method: a general procedure of protein complex purification. Methods *24*, 218-229.

Rodriguez-Gil, A., Garcia-Martinez, J., Pelechano, V., Munoz-Centeno Mde, L., Geli, V., Perez-Ortin, J.E., and Chavez, S. (2010). The distribution of active RNA polymerase II along the transcribed region is gene-specific and controlled by elongation factors. Nucleic Acids Res *38*, 4651-4664.

Selitrennik, M., Duek, L., Lotan, R., and Choder, M. (2006). Nucleocytoplasmic shuttling of the Rpb4p and Rpb7p subunits of Saccharomyces cerevisiae RNA polymerase II by two pathways. Eukaryot Cell *5*, 2092-2103.

Shannon, P., Markiel, A., Ozier, O., Baliga, N.S., Wang, J.T., Ramage, D., Amin, N., Schwikowski, B., and Ideker, T. (2003). Cytoscape: a software environment for integrated models of biomolecular interaction networks. Genome Res *13*, 2498-2504.

Simon, J.L. (1997). Resampling: The New Statistics. (Arlington, Virginia, USA., Resampling Stats, Inc.).

Thompson, N.L., Lieto, A.M., and Allen, N.W. (2002). Recent advances in fluorescence correlation spectroscopy. Curr Opin Struct Biol *12*, 634-641.

Zenklusen, D., Larson, D.R., and Singer, R.H. (2008). Single-RNA counting reveals alternative modes of gene expression in yeast. Nat Struct Mol Biol *15*, 1263-1271.

Supplemental Figure 1

Click here to download Supplemental Figure: Haimovich fig S1 reduced size.pdf

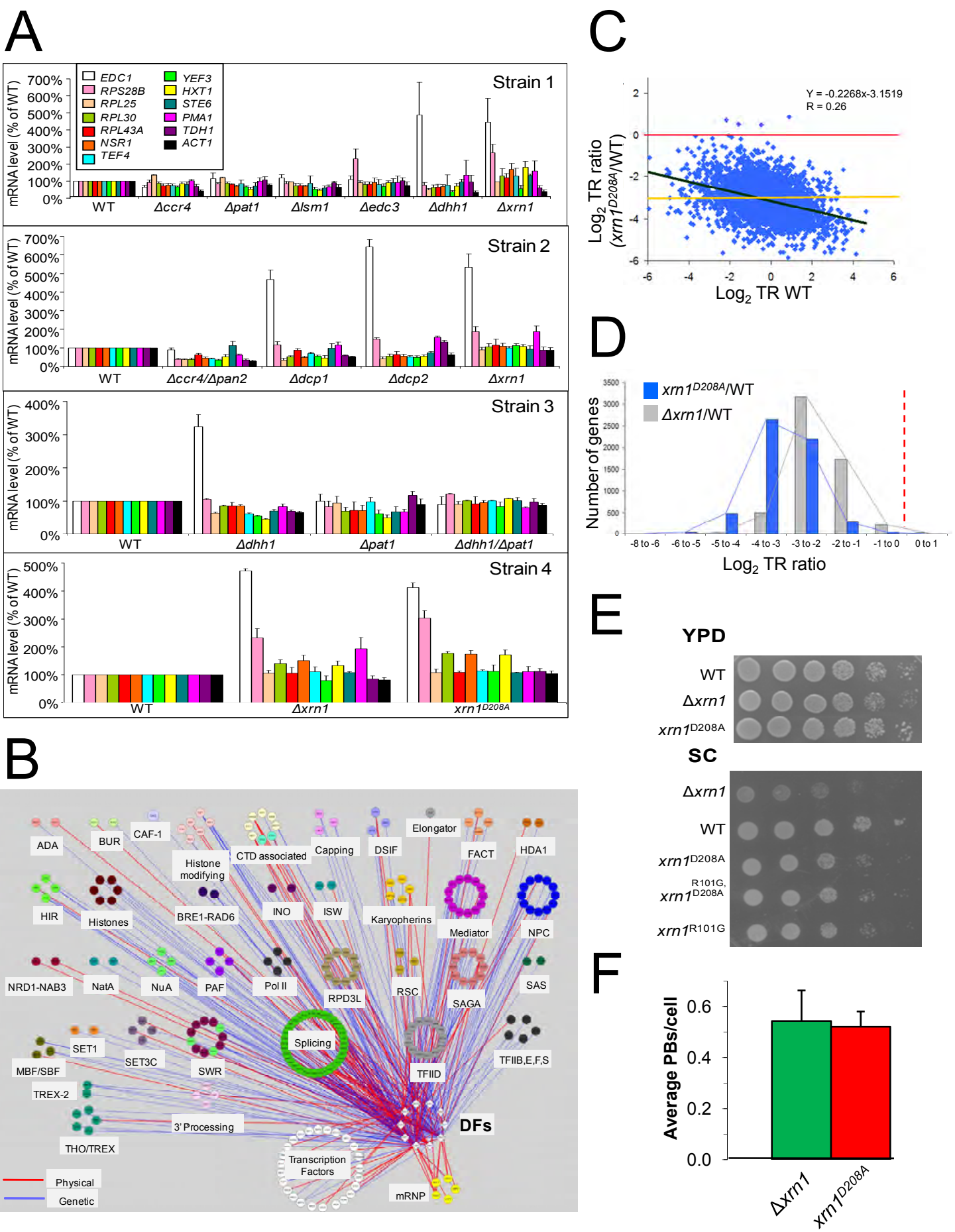

Supplemental Figure 2

Click here to download Supplemental Figure: Haimovich fig S2 reduced size.pdf

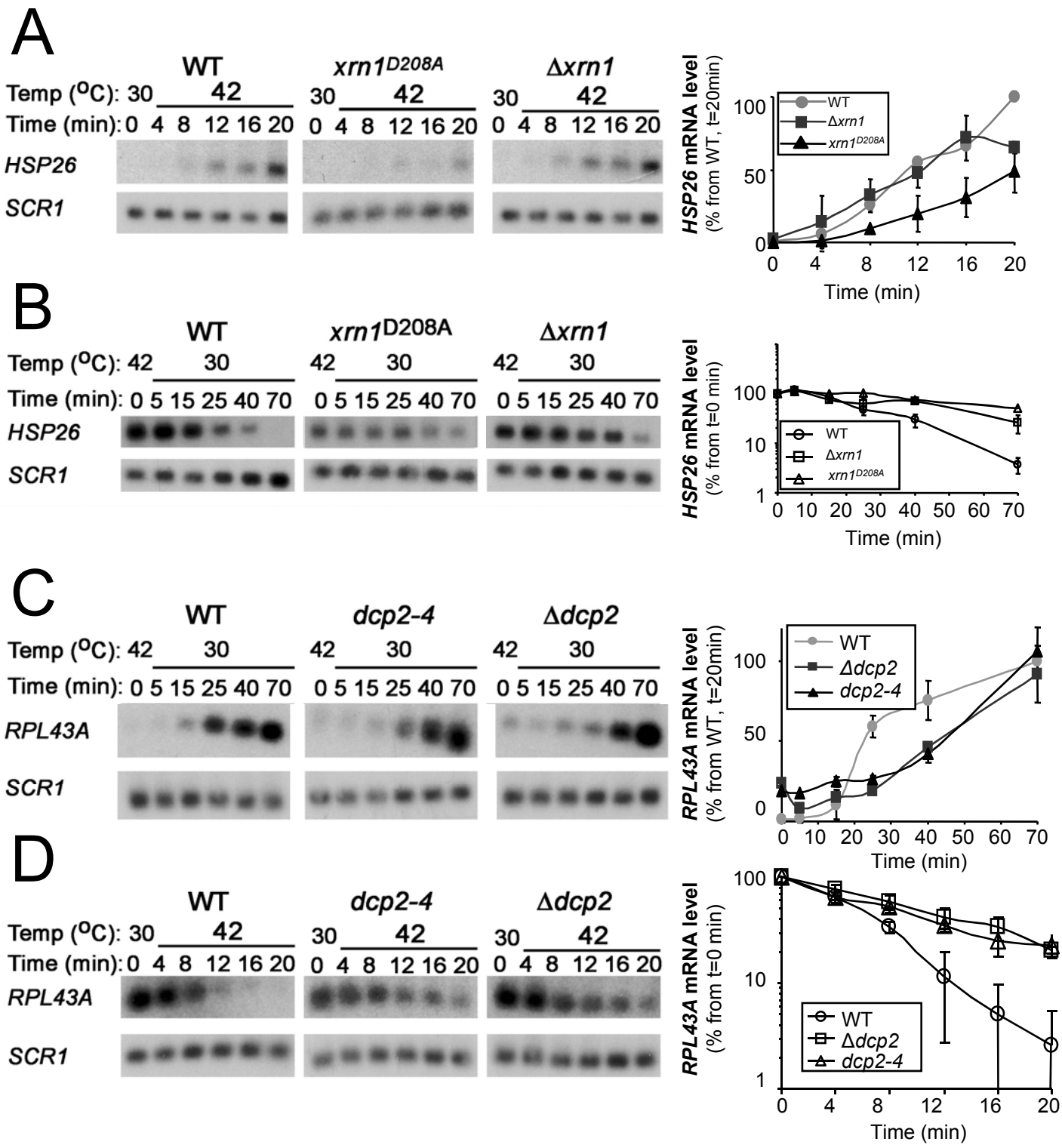

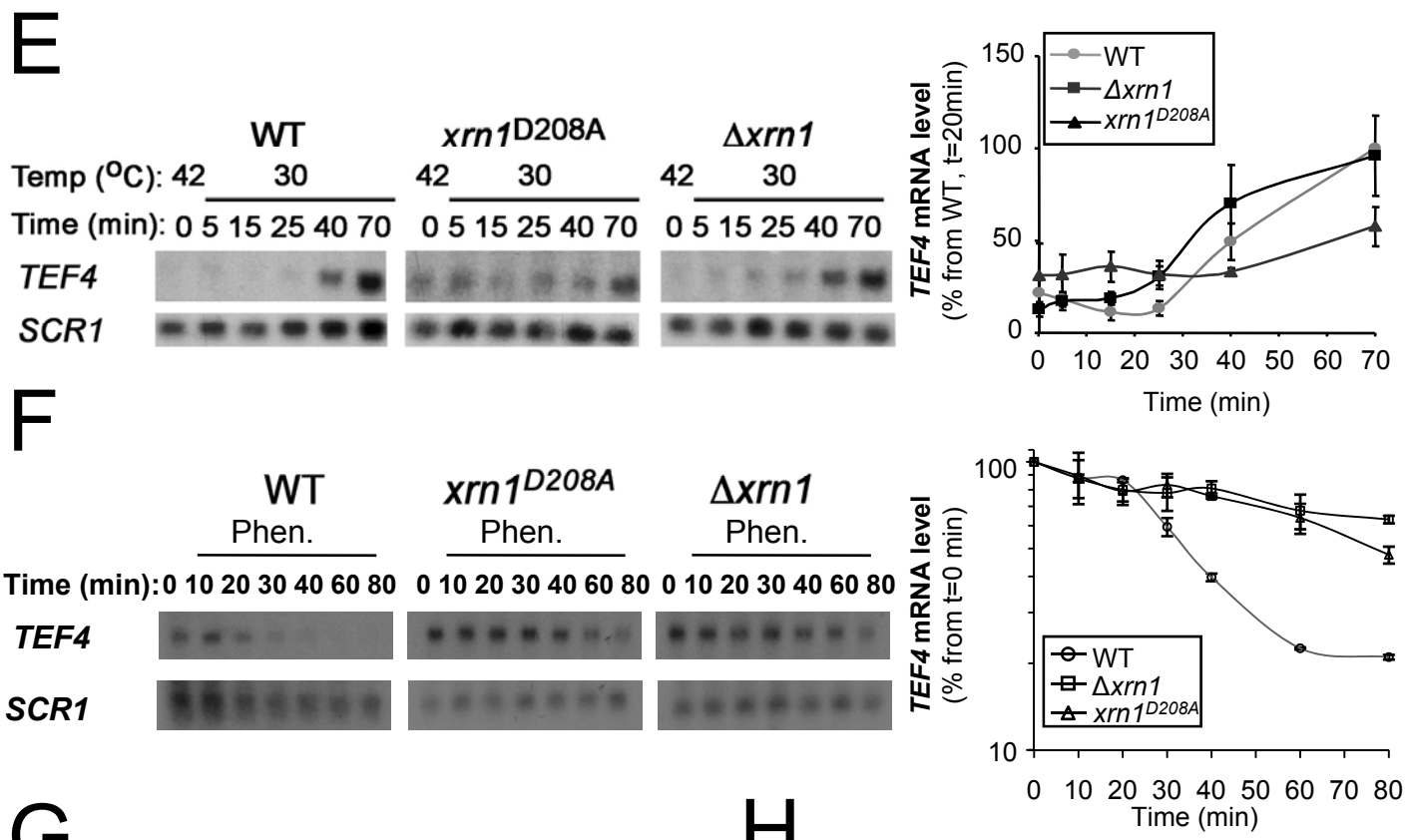
E
WT
xrn1D208A
Δxrn1
Temp (°C): 42 30 42 30 42 30
Time (min): 0 5 15 25 40 70 0 5 15 25 40 70 0 5 15 25 40 70
TEF4
SCR1
TEF4 mRNA level (% from WT, t=20min)
WT
Δxrn1
xrn1D208A
Time (min)
F
WT
xrn1D208A
Δxrn1
Phen.
Time (min): 0 10 20 30 40 60 80 0 10 20 30 40 60 80 0 10 20 30 40 60 80
TEF4
SCR1
TEF4 mRNA level (% from t=0 min)
WT
Δxrn1
xrn1D208A
Time (min)
G
WT
dcp2-4
Temp (°C): 30 42 30 42
Time (min): 0 4 8 12 16 20 0 4 8 12 16 20
SUT508
SCR1
H
WT
dcp2-4
Temp (°C): 42 30 42 30
Time (min): 0 5 15 25 40 70 0 5 15 25 40 70
SUT508
SCR1
I
WT
Δpat1
Δdhh1
Phen.
Time (min): 0 10 25 50 80 0 10 25 50 80 0 10 25 50 80
**
SUT508
*
SCR1

Supplemental Figure 3

Click here to download Supplemental Figure: Haimovich fig S3 revised.pdf

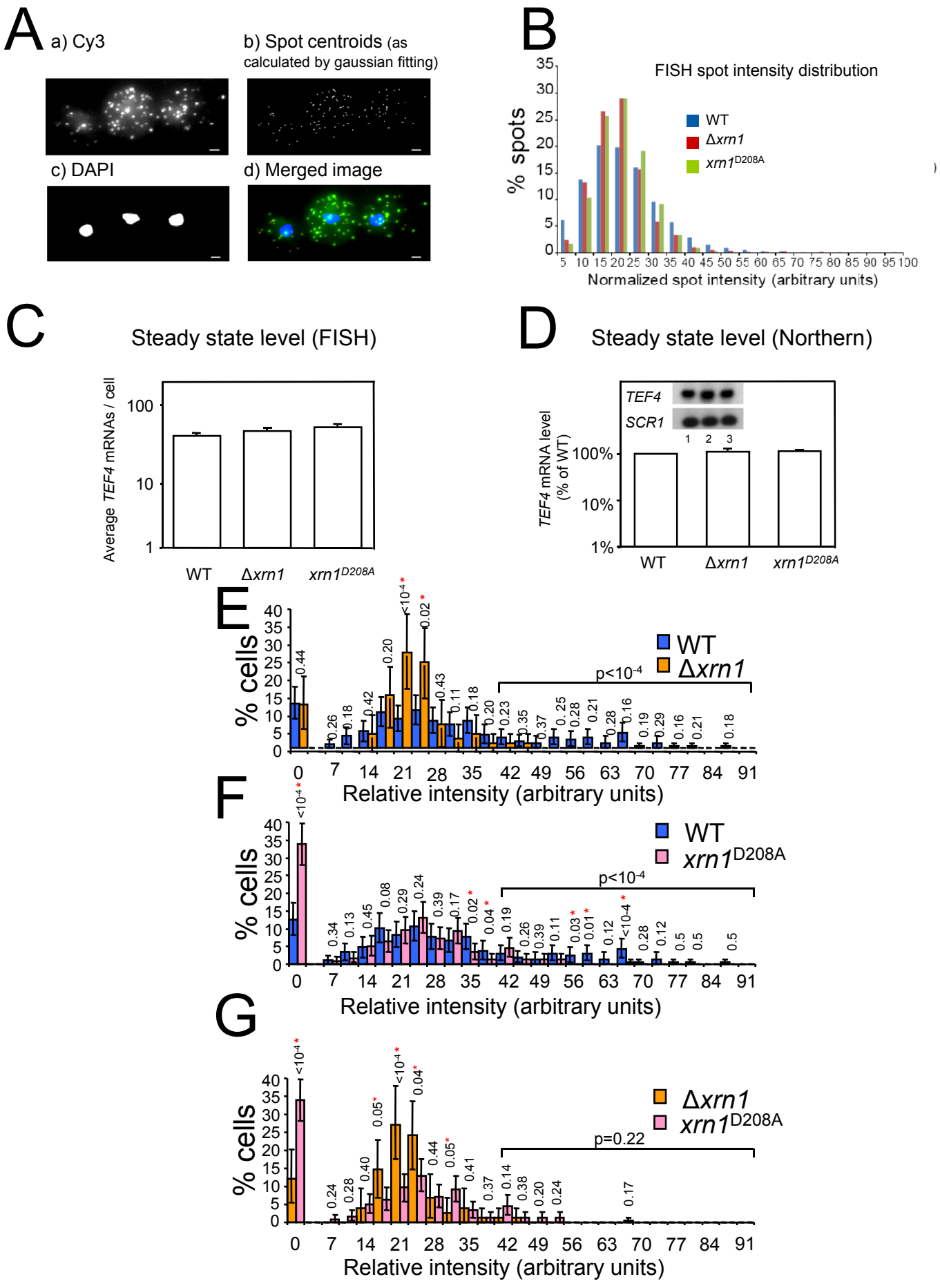

Supplemental Figure 4

Click here to download Supplemental Figure: Haimovich fig S4 reduced size.pdf

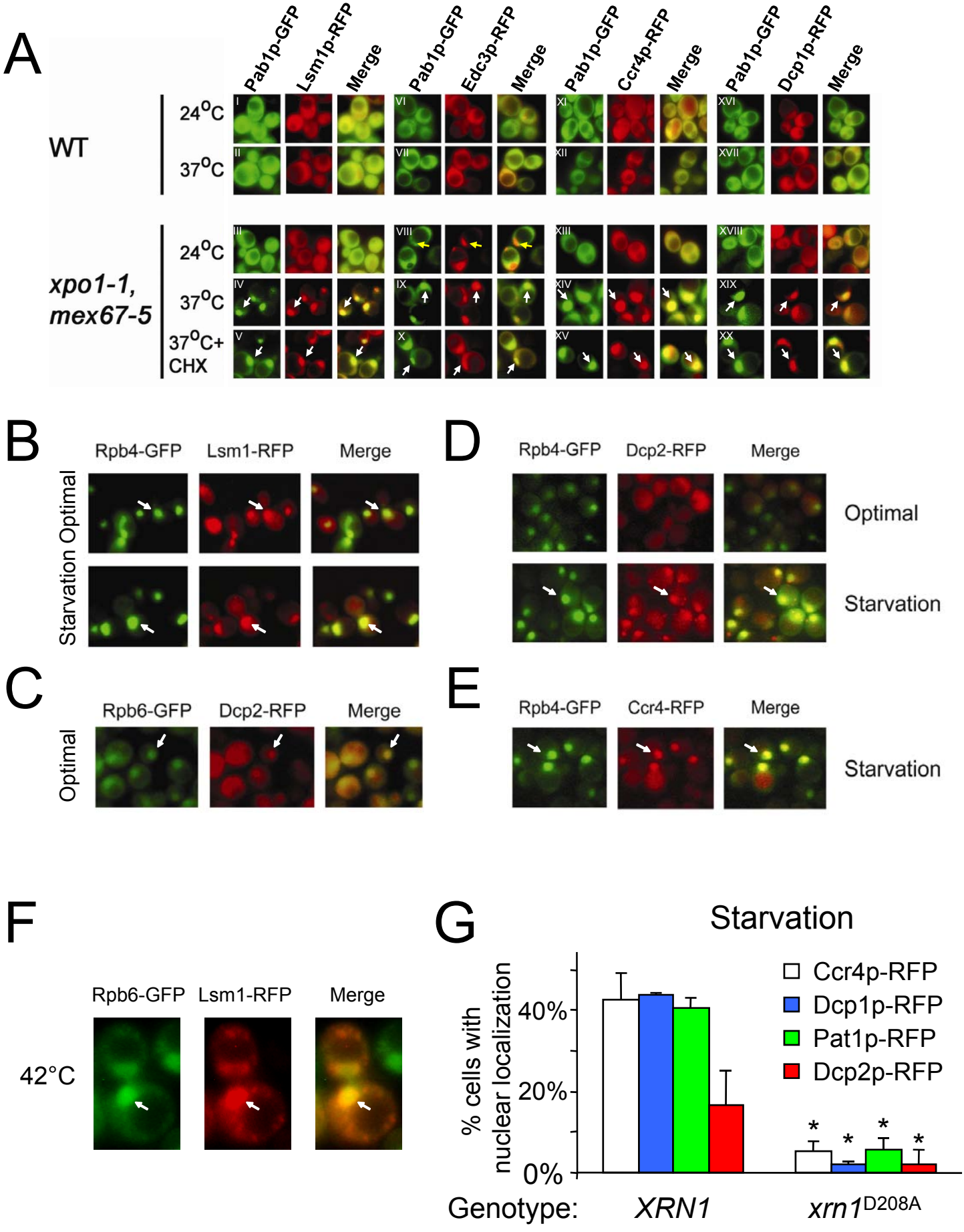

Supplemental Figure 5

Click here to download Supplemental Figure: Haimovich fig S5_revised_20_2_12 gal.pdf

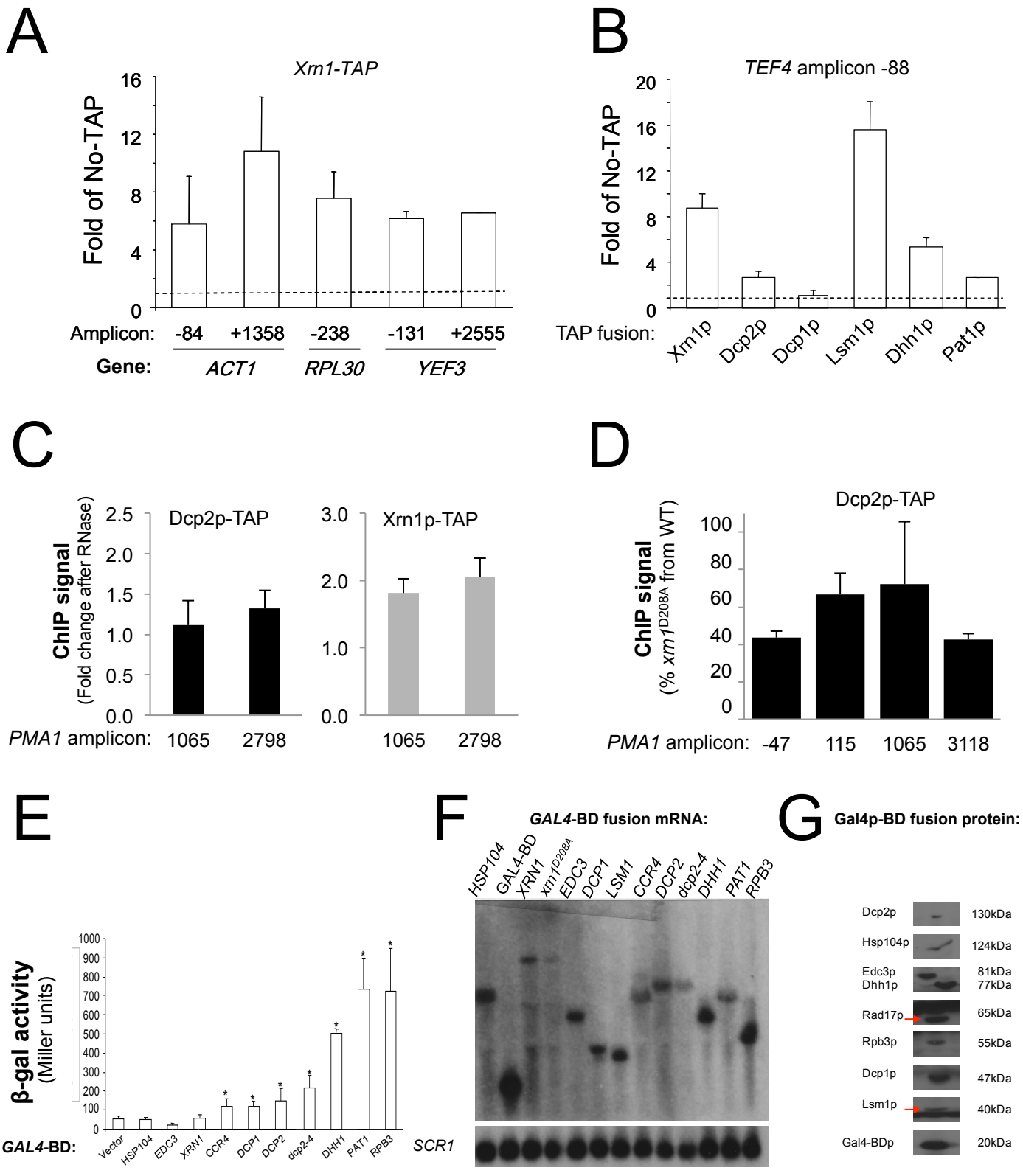

Supplemental Figure 6

Click here to download Supplemental Figure: Haimovich Fig S6 14_2_12.pdf

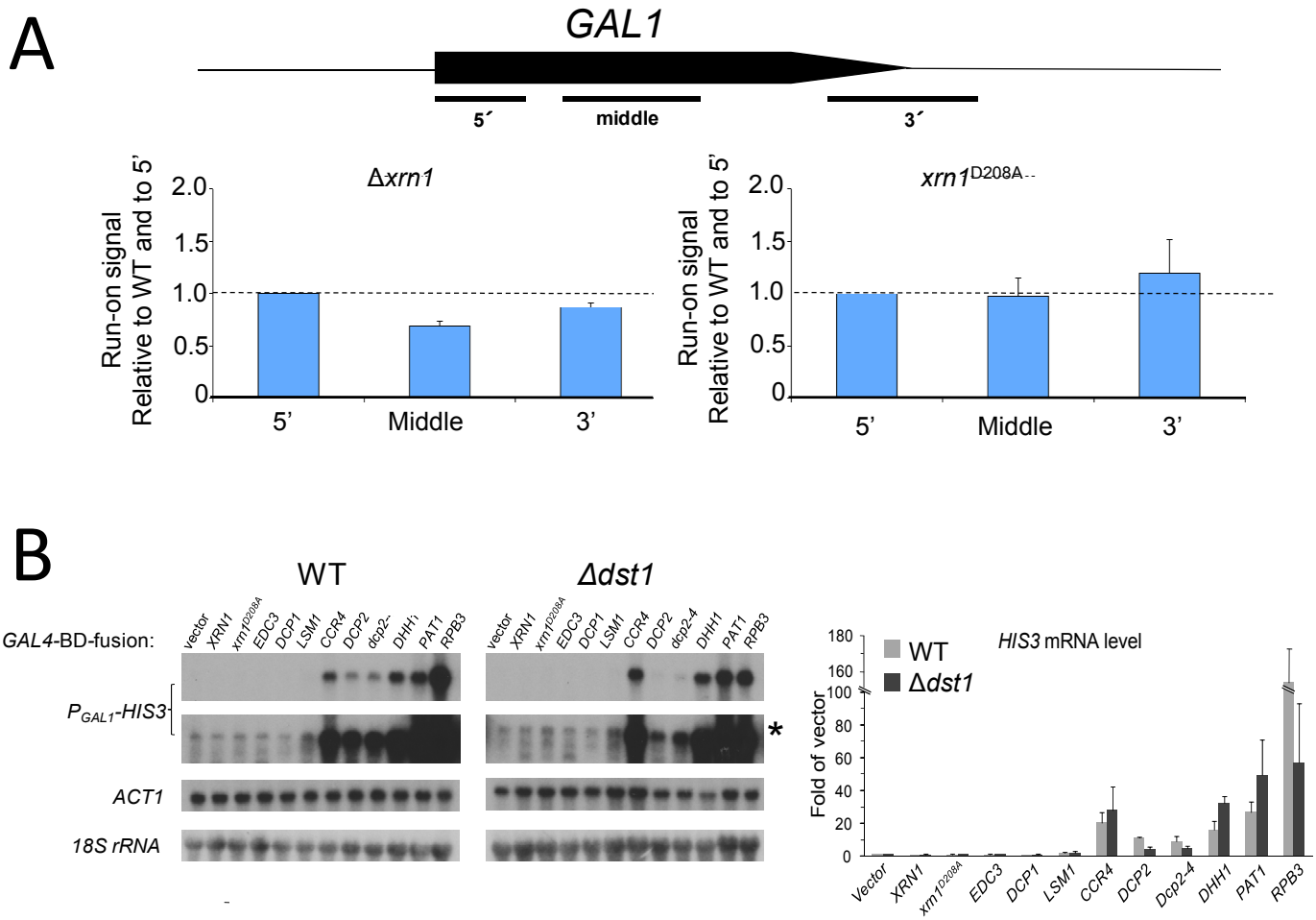

Table S1

Click here to download Supplemental Movies and Spreadsheets: Table S1 (delta).xls

Table S3

Click here to download Supplemental Movies and Spreadsheets: Haimovich Table S3[1].xls

Table S4

Click here to download Supplemental Movies and Spreadsheets: Table_S4[1].xls

Supplemental Movie S1

Click here to download Supplemental Movies and Spreadsheets: HaimovichMovieS1.avi

Supplemental Movie S2

Click here to download Supplemental Movies and Spreadsheets: HaimovichMovieS2.avi

Supplemental Movie S3

Click here to download Supplemental Movies and Spreadsheets: HaimovichmovieS3.avi

Supplemental Movie S4

Click here to download Supplemental Movies and Spreadsheets: HaimovichMovieS4.avi